Design, implementation, and qualification of high-performance time and frequency reference for the MeerKAT telescope

Johan Petrus Burger,[a,*] Renier Siebrits,[a] Romeo Reginald Gunther Gamatham,[a] Geomarr van Tonder,[a] Grant Adams,[b] Vereesé van Tonder,[b] Zwivhuya Ramudzuli,[b] Sarah Buchner,[c] Michel Abgrall,[d] Pierre Uhrich,[d] and Daniele Rovera[d]

[a]South African Radio Astronomy Observatory, Time and Frequency Systems Group, Engineering Division, Cape Town, South Africa

[b]South African Radio Astronomy Observatory, Electronics Group, Engineering Division, Cape Town, South Africa

[c]South African Radio Astronomy Observatory, Commissioning and Science Group, Science Division, Cape Town, South Africa

[d]LNE-SYRTE, Observatoire de Paris, Université PSL, CNRS, Sorbonne Université, Paris, France

Abstract. The details of the MeerKAT radio telescope's time and frequency reference subsystem that enables sampling via low-jitter, low-drift microwave clock signals, and absolute timing (≤5 ns accurate) are discussed. The subsystem's microwave and pulse per second transmission parts are now fully qualified and commissioned for the ultra high frequency (UHF) and L-bands and also provide for a 100-MHz interface and timing interfaces for S-band receivers that were installed. The subsystem includes a cable measurement system called the Karoo array timing system (KATS). Performance and differences on different bands and seasonal drift of the cable delay measurement of KATS are reported. A time scale called the Karoo Telescope Time (KTT) (which is estimated from tracking a few atomic clocks via new software) and the issuing of timing bulletins to users have been largely implemented and verified. Absolute timing calibration and linkage of KTT to the global positioning system time scale and to different UTC(k) realizations of the Coordinated Universal Time (UTC) instances are described. The subsystem uniquely enables high-fidelity sampling and stable tied array configuration. The latter configuration enables timing and transient science over time spans of 5 to 10 years. Simultaneous subarraying is supported. The backend is unique for radio telescopes in terms of being very deterministic as far as timing is concerned. [DOI: 10.1117/1.JATIS.8.1.011013]

Keywords: MeerKAT; radio; telescope; time transfer; calibration.

Paper 21102SS received Aug. 31, 2021; accepted for publication Dec. 7, 2021; published online Jan. 11, 2022; corrected Jan. 21, 2022.

1 Introduction

The time and frequency reference (TFR) for a phased array telescope ensures that all the data collected at the separated receivers are coherent, and that the absolute timing is known at each receiver. The TFR consists of an ensemble of atomic clocks, microwave upconversion synthesizers, and transmission equipment to supply a sample clock to the radio receiver digitizers. Global Navigation Satellite System (GNSS) tracking, network protocol, and pulse per second (PPS) timing transmission equipment, as well as true time delay measurement apparatus for connecting to digitizing equipment up to 12 km away from the central digital signal processing and computing building (called the Karoo Array Processor Building or KAPB) are described.

*Address all correspondence to Johan Burger, jburger@sarao.ac.za

The 64 antenna (offset Gregorian reflector type) phased array MeerKAT ("more of KAT"; KAT is the Karoo Array Telescope) radio telescope[1] (and its extension) is a new generation cm wavelength radio telescope that has been built in South Africa. It has been performing high-fidelity imaging[2,3] that also resulted in the discovery of giant radio galaxies.[4] Photometric, spectrometric, and polarimetric studies can be done in conjunction with optical telescopes including the South African Large Telescope and a smaller robotic telescope (MeerLICHT) that follows MeerKAT's field of view.[5] An important design goal, which is to perform time domain science, has been largely achieved due to the relatively compact core and recent promising observations.[6–8] Some pulsars' stability of the order of 4 ns $\cdot$ h^{-1} is now projected based on MeerKAT measurements.[9] This is an improvement of prior best state-of-the-art measurements on the Parkes Pulsar Timing Array in 2014.[10] The MeerKAT (and its current extension to an 80 antenna array[11–13]) serves as a precursor for the 133 antenna square kilometer array (SKA) mid-frequency phased array telescope.[14]

Radio frequency interference (RFI) suppression is important due to the presence of very sensitive cryogenically cooled receivers with a noise temperature of between 5 and 6.5 K for the SKA band 2 receivers (0.95 to 1.76 GHz).[15] The digitizers are separated by mere meters from these receivers in the desert air, and the time and frequency interface is a module in the digitizer, called the sample clock generator (SCG). The SCG can receive and reflect RF modulated PPS and receive a sample clock over optical fiber. The digitizer converts the timing signal into the flagging of a single bit at the right epoch. The L-band bit period is <600 ps. The relative inter-antenna sample clock timing/phase is far more precise after phase-up of the telescope, due to digital signal processing techniques used in the correlator. This interferometric phase-up also means that absolute timing registered at a number of antennas can be transferred to other antennas with an accuracy of a few ps. Preliminary results related to the subsystem[16,17] and a brief introduction of the TFR were previously given in a journal paper on pulsar science[6] and new results are discussed in this manuscript. It was previously shown that sub-100-fs jitter and ≤1 ps drift were reported for the sample clock after the photoreceivers used in the MeerKAT and sub-30-ns tracking were achieved. The latter time tracking uncertainty with respect to the Coordinated Universal Time (UTC) is now reduced to the ∼5 ns level.

The flow of this paper is structured as follows:

(a) The user requirements, science drivers, and resulting systems requirements for this telescope subsystem are discussed in Sec. 2.

(b) The design and implementation to realize such requirements are shown in Sec. 3.

(c) Thereafter, sections on the measurements and characterization and analysis of results prove that the parts of system meet the requirements in Secs. 4–6.

Ongoing work is mentioned in Sec. 7, and then there is a discussion and conclusion on what was achieved in Sec. 8. This discussion has a larger emphasis on the timing accuracy verification, which is the newer result in part (c), and therefore much detail on that is shown explicitly in Sec. 6, which is supported by further analysis in Appendix A.

2 Key User Requirements, Science Drivers, and Summary of Main Requirements

2.1 *Key Timing Requirement and Science Drivers*

The important variables for a phased array like MeerKAT are the timing accuracy at the antennas and phase stability and jitter of the radio frequency (RF) sampling clock. Furthermore, network time in the form of Precision Time Protocol (PTP) Ethernet packets that are widely supported by mainstream equipment is required. The MeerKAT user requirements are such that it is an octave spanning fully polarimetric and spectroscopic instrument in the ultra high frequency (UHF), L, and S bands. MeerKAT is also capable of doing very long baseline interferometry (VLBI) with external telescopes in similar bands.

Imaging and timing modes are used in the study of objects such as magnetars,[18] and phase stability is important to reach high signal-to-noise ratio and high contrast (in imaging and time

domain science). Signal-to-noise ratio in signal chains are, amongst other things, affected by jitter[19] and the effect of phase stability on coherence loss is well known as described in Ref. 20. This potential coherence loss is also important in VLBI, and MeerKAT had to have such capability, which is virtually assured by the usage of a maser, due to masers' stability.

Approximately half of MeerKAT's observation time has been allocated toward pulsar observations and fast radio transients. Pulsar and transients science is a rich field, in which much contemporary physics and astrophysics questions may be answered, and there is the long-mentioned possibility of gravitational wave detection via timing.[21] The discovery of a close-pair binary in a supermassive black hole system has raised the possibility of detecting gravitational waves from black-hole interactions.[22] Furthermore, pulsar dynamics may be changed by being in the vicinity of black holes,[23] which is part of the reason for an intense search to find pulsars in the vicinity of black holes.[24–26] Accurate timing on the telescope backend might conceivably allow pulsars to be used for telescope-based solving of position,[27] which have some similarity to using such sources for interplanetary navigation.[28] This opens up the possibility to further studies in geophysics, apart from determining and improving error in the planetary ephemeris.[29] MeerKAT can observe up to four pulsars simultaneously with accurate timing, by using subarrays.

From a timing perspective, a key user requirement was that under normal operating conditions the telescope instrumental effects, excluding time stamping, shall not limit the achievable pulsar timing accuracy to worse than 10 ns RMS. If one has a source of 5 ns inherent jitter and one has 5 ns instrumental noise in timing, one can reach 7 ns of timing uncertainty. This was of the order of pulsar sources' timing uncertainty that might be found and half of the projected source limitations[10] at the time. There was also a realistic outlook that some pulsar fluctuations might be better understood with further study.[30] Phase noise requirements were established from a telescope analysis process and apportionment of telescope level requirements to subsystems including the TFR using standard systems engineering methodology.[31]

The user-required onsite time stamping accuracy of a 1-ns level that was specified at telescope level,[31] was relaxed. This low level could have required higher-accuracy atom clocks for onsite monitoring and/or two-way satellite time and frequency transfer (TWSTFT).[32] Due to the complexity and cost, the requirement was enlarged to the more realistic $\leq$5 ns level.[33] Regular TWSTFT is incompatible with onsite RFI requirements; in 2019, only about 12 timing laboratories could use TWSTFT, likely due to cost and complexity.[34] It was calculated that tracking with a 5 ns accuracy could be achieved according to an uncertainty budget using maser and dual-frequency GNSS geodetic receivers. At the time requirements were set in 2013/2014, low-noise methods of time transfer with low local RF emissions like with the precise point positioning (PPP)[35–37] were still under development, and it was hard to reach offset calibration accuracy approaching 1 ns. The local accuracy would be limited by the time transfer to other laboratories, and calibration offsets did not reach the low values that are currently seen in the top laboratories.

Existing VLBI installations of the South African Radio Astronomy Observatory (SARAO), such as at the Hartebeeshoek Radio Observatory (HartRAO), in fact used somewhat noisy single-frequency GPS derived timing pulses[38] to track its time. It was clear that improved GNSS methods would have to be used for MeerKAT. Nonetheless, high-availability requirement of the telescope meant that reliable active hydrogen maser-type technology, which had proven radio science credentials, was chosen over more contemporary clock types because, among other reasons, it enables VLBI[39] by having enough stability to ensure high coherence between radio receivers clocked by individual masers separated by 1000's of km. A room of $\sim 5 \times 5$ m^2, in an already crowded data rack area, could be obtained for the clocks and clock monitoring equipment. Another room of $\sim 5 \times 2.5$ m^2 was obtained for six racks to be used for transmission, of which three were utilized by MeerKAT and three allocated to the mid-frequency square kilometre array (SKA-MID)[14] radio telescope.

2.2 *Accuracy in Time of Arrival and Determinism in Telescope Backend*

The accuracy of the backend of a whole telescope is challenging as it is a distributed instrument and there is no technology that can herald a single accurate time at the central processing facility. All systems, including the Karoo array timing system (KATS), must either measure or compensate for cable changes and careful calibration of each link in between parts of the telescope are

needed. There are always differences measured in each link with respect to a true time difference, and one simply tries to minimize the residuals. All known systems must have accurate tracking against the UTC, which is also known only *post facto* after the publication of the Bureau International des Poids et Mesures (BIPM) Circular T. To do time-tagging at the 5-ns level at a telescope level, one requires an absolutely calibrated backend. Our work expands on earlier work on the Parkes Pulsar Timing Array, which revealed variable timing delays[40] and which shows that even on a single antenna, this is no trivial task. In the MeerKAT telescope, hardware delays were carefully measured in the whole clock system, and there are specialized time transfer links to the antennas that use a traceable method.[41] The PPS from the Karoo Telescope Time (KTT) is distributed to the different antennas via modulated RF on an optical carrier, and part of it is optically reflected in digitizers to measure the round-trip delay to the digitizers.

2.3 *Engineering Requirements*

The key TFR performance requirements are listed in Table 1 in an abbreviated form. The first requirement deal with the fidelity of tracking the clocks with respect to UTC. Furthermore, time is disseminated by a PPS, and cables are measured by the KATS method, and the time of arrival has to be deterministically known with an uncertainty below 1.6 ns. The system also has to be able to support four subarrays, and multiple points are also needed in each subarray to be able to statistically detect timing outliers. In order to detect outliers and have a small number of detection points, a total number of 19 KATS ports were realized per band,[42] so that four or five simultaneous measurements are possible per subarray. This reflects that no system has perfect heralding of time across a subarray, and that some statistical sorting and handling of time sensors are needed in a distributed system like a radio interferometric array. Precise sub-2-ns timing is not required at each and every antenna for the reason that time is disseminated in an interferometric array via

Table 1 Summary of key functional and performance requirements for the TFR.

Requirement name	Requirement description
Uncertainty allocation for telescope time	The tracking uncertainty of the TFR system time realization (KTT) shall be ≤5.0 ns RMS with respect to the UTC as published in the BIPM Circular T after accounting for the master clock offset with respect to UTC
Uncertainty of fast precision time feed-in (PPS) via KATS	The offset corrected time transfer from the TFR shall take place between the TFR and the digitizer with uncertainty ≤1.6 ns RMS as measured between the output of the TFR clock system and the digitizer
TFR subarraying and tied array support	The TFR shall be able to support at minimum 16 digitizers via KATS, simultaneously, also provide this KATS to at least four subarrays simultaneously, and do this in a redundant manner
Short-time scale RMS phase requirement (L-band)	For timescales shorter than 1 s, the RMS of the period variation of the RF sampling clock in the optical domain at the output of TFR shall be ≤9.5 ps
Long-time scale RMS phase requirement (L-band)	The period variation of the sample clock over time scales of 1 s to 20 min (after subtraction of a linear fit over 20-min intervals) shall be ≤12.5 ps RMS, when separate masers and separate optical transmission systems are used
Maser and synthesizer jitter	The TFR clock jitter at the output of a synthesizer at the KDRA for any frequency band shall be ≤50 fs RMS, integrated from 1 Hz to 100 MHz carrier offset
Other jitter contributors	All other contributors to the jitter, as measured after the RF sampling clock synthesizer to the ADC on the digitizer, excluding the fiber itself, shall add ≤160 fs RMS in a 1-Hz to 100-MHz carrier offset
Method of distribution of network time	Time shall be distributed over an Ethernet network using the PTP protocol
GPS steering of network time	The TFR network portion shall synchronize its own time to within 10 μs (RMS) of UTC from within 1 h of startup of the TFR, via GPS

phase up of the array via correlation methods. If the time at a single antenna has been robustly determined via comparison with measurements at a few other antennas, the time from that antenna is effectively transferred to the rest of the array that does not need such precise measurement points. It has been found that there is good phase stability (low drift), several hours after phase up on a stellar calibrator. There is still synchronization taking place via a PPS to the digitizers: there are counters on the digitizers that are software configurable.

The TFR also provides sampling clocks to the digitizers that are situated on the indexers of the antenna positioners. In MeerKAT, the microwave sampling clocks are centrally distributed for L and UHF-bands and the system is simplified using buried fiber cable to reach the required phase stability. The centrally distributed clock is filtered at the digitizers with filters with a bandwidth of 20 MHz.

The PTP is used for transmission of network time[43] that is used in devices that needs time (other than the digitizers, which must use the high-precision PPS). The PTP is widely supported by network switch suppliers, and high-performance versions can supply $\leq$5 ns uncertainty in timing.[44] The PTP can operate together with data and control and monitoring packets on a network and does not need special dedicated fiber for doing such. The network loading of this protocol is low, and the packets can co-exist with the transmission of commands, control and data.

The telescope clock timing needs to be tracked against the UTC, which is accomplished through GNSS receivers. Our science requirement is to produce timing on a 15-min period and not 5 days as obtained in the UTC calculation, and furthermore, we also must produce clock file bulletins that supply the difference between the KTT and the UTC (or a close enough prediction of UTC to fulfill uncertainty requirements). Our clock file is published every 2 weeks as opposed to the BIPM Circular T, which is published monthly. In principle, tracking can take place against high-quality UTC nodes standards, and in this work, a comparison is done against the predictions and corrections done by the laboratory Système de Références Temps-Espace (SYRTE) at the Observatoire de Paris (OP), designated by the French National Metrology Institute Laboratoire National de Métrologie et d'Essais (LNE) for time and frequency metrology activities, apart from earlier comparison work against the National Metrology Institute of South Africa (NMISA). It was a stated goal in 2014 that GNSS tracking should include PPP, and such work was performed together with the LNE-SYRTE.

3 Overall System Description and Physical Implementation

3.1 *System Overview*

An overview of the MeerKAT time and frequency system is shown in Fig. 1.

The MeerKAT time and frequency system consists of two T4Science iMaser 3000 hydrogen masers and two Spectracom GPS steered rubidium atomic clocks. The hydrogen masers are monitored against the GPS time using dedicated Septentrio PolaRx4TR GNSS time transfer receivers. The GNSS time transfer receivers are directly attached to the masers to avoid series component reduction in reliability in tracking[45]; at this stage, it has a negligible effect on the system uncertainty, as shown in Appendix A. The clocks are also monitored against each other using Keysight 53230A time interval counters (TICs). TICs are also used to continuously measure the Septentrio GNSS receiver's internal delay, which refers to the delay from the PPS input to the internal latching point of the PolaRx4TR. A clock selector selects which of these four clocks currently provides the reference signals to the MeerKAT. The clock selector provides the capability to remotely switch between clocks should any problems arise on any of the clocks. The GPS steered rubidium clocks also serve as PTP time servers/grand masters to provide PTP timing packets to the antenna control units (ACUs) located at the antenna pedestals. The advantage of PTP compared to other time transfer algorithms is that it achieves the required accuracy and also has a basic fail-over capability called the best master clock algorithm.[46] The PTP performance was tested at the ACUs and in terms of timing accuracy (it is $\sim$250 ns for MeerKAT limited by the test equipment[47]) and fail-over capability. The ACU did implement a software PTP stack in order to assist in the steering of the antennas and easily gets to the requirement specification of <1 ms compared to a PTP slave clock that was used in the measurement of the antenna, in a time of <1 min.[48] The

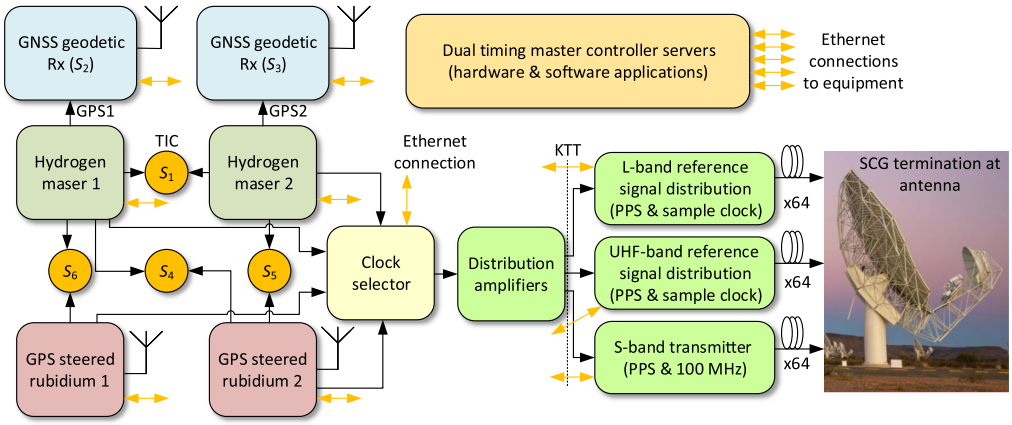

Fig. 1 A high-level overview of the MeerKAT time and frequency system. The masers are tracked via geodetic GNSS receivers that are called GPS1 and GPS2. The system is interconnected to the timing monitoring and control (TMC) servers through an Ethernet network. The yellow double-sided arrows indicate data transfer and communication with the TMC. The sample clock and PPS are transmitted through 64 individual fibers to antenna positioners, in which the digitizers are mounted at the indexer. The digitizers contain a module called the SCG, which is the point of reception for the TFR signals, except for a portion of the RF modulated PPS that is reflected back to the transmitters for measurement. Several devices produce datastreams S_i as shown in this figure, and these data are used in fused multisensor clock tracking as described in Sec. 3.6.2. The datastreams S_2 (timing differences from maser 1 called SKA1 to GNSS satellite clocks) and S_3 (timing differences from maser 2 called SKA2 to GNSS satellite clocks) as generated by the two geodetic receivers GPS1 and GPS2 are two important parts of this.

basic phase noise requirement was fulfilled using Rhode and Schwarz SMA-B103 RF synthesizers with the low close in phase noise option SMAB-B710N and placing it in the maser room for temperature and therefore phase stability. There is some low residual phase noise, and this was characterized and found to conform to requirements. This is discussed in Sec. 4.1.

The masers are also compared to each other using a Microsemi 5120A Dual-Mixer Time Difference (DMTD) apparatus. Most errors on any maser can be picked up via the TICs (since there are four clocks that are compared to each other) and via evaluation of the timing sensor parameters' values S_i as per Fig. 1.

3.2 *Physical Infrastructure and Special Measures Taken to Ensure System Requirements Are Met*

The masers, GPS rubidium clocks and clock monitoring equipment, and synthesizers are placed inside a maser room inside the KDRA, which is temperature controlled to 24°C ± 2°C via two precision lab air-conditioning units made by Climaveneta. The temperature is such that it conforms to the calibration temperature of precision Septentrio PolaRx4TR and PolaRx5TR time transfer GNSS receivers. The masers are enclosed inside special Peltier cooled thermal enclosures, which further reduces the temperature variation on the masers to ∼ ± 0.2°C. The masers are placed on damping surfaces consisting of Thorlabs stainless steel optical tables and dampers with feet that sit on a large metal plate to distribute the weight on the bottom screened floor, and new custom fans were put into the masers in place of the standard fans to further reduce residual vibrations.

Electrical supply redundancies are built in for very high availability. The KAPB provides two dedicated, three-phase power lines to the TFR rack area. Each rack has a static transfer switch to smoothly fail-over between these two power lines in the event of a partial power failure. A large battery UPS is dedicated to the power backup of all masers and clock monitoring equipment and the air conditioning for the maser room, apart from separate smaller UPSs for the masers and the monitoring equipment. In addition, each rack with transmission equipment has an interactive UPS, which has sufficient capacity to ensure the automatic shutdown of sensitive signal distribution equipment in the event of a complete power failure. There is a plug point and automatic

power fail-over panel near the KDRA entrance to power the TFR system from separate diesel generators in case of power failures. Special measures were also taken to eliminate effects of the low-humidity KDRA air, which can cause effects on many of the clocks and transmission equipment via electrostatic discharge (ESD) interference with equipment.

3.3 *Control, Monitoring, and Sensors*

The TFR's TMC subcomponent, consisting of both several pieces of hardware and software, is responsible for the monitoring and control of the TFR system. The TMC makes use of the Karoo Array Telescope Communication Protocol[49] for communication between hardware and the software needed for control and monitoring. The TMC actually consists of several computers and several types of software deployed on it: that is, two ruggedized servers that operate in a redundant manner and are connected to industrial Ethernet switches supporting the PTP. In the maser room, there are two fanless computers that communicate with the ruggedized network switches. Interim data are stored on the fanless computers, should there be issues on the other computers and the rest of the network. There are a large number of environmental sensors, and equipment linked to the thermoelectric heat exchangers of the maser heater cooler boxes. All the instrumentation and monitoring equipment are connected to Ethernet interfaces and can therefore communicate through Ethernet switches with the servers of the TMC. At this stage, the TMC also monitors a number of associated supporting infrastructure items, so that the total number of sensorized data streams approaches 2000. The TMC and all its software and how it relates to clock tracking will be discussed in further publication(s).

3.4 *Transmission System Implementation*

3.4.1 *Overall description of the reference/sample clock signal distribution*

The MeerKAT reference signal distribution system consists of distribution systems for in-house developed L- and UHF-band systems as well as the S-band receivers and its associated TFR generator supplied by the Max Planck Institute for Radio Astronomy. The sample clock transmitter and PPS transmitter are responsible for distributing the analogue-to-digital (ADC) sampling clock signal and PPS signals from the TFR inside the KDRA to the digitizers mounted on the antennae. A description of the L-band distribution system is available in Ref. 17. Note that the PPS transmitter and KATS systems both distribute PPS; however, KATS has the additional functionality to measure the round-trip delay to a digitizer on the indexer. This measurement is used to determine the timing offset of a specific digitizer from KTT. This functionality is only required for antennas in the core of MeerKAT, which are mainly used for the timing of pulsars. Four of the L-band KATS ports are also connected to 4 of the S-band receivers to determine their timing offset from KTT. An overview of the reference signal distribution for the MeerKAT telescope is shown in Fig. 2.

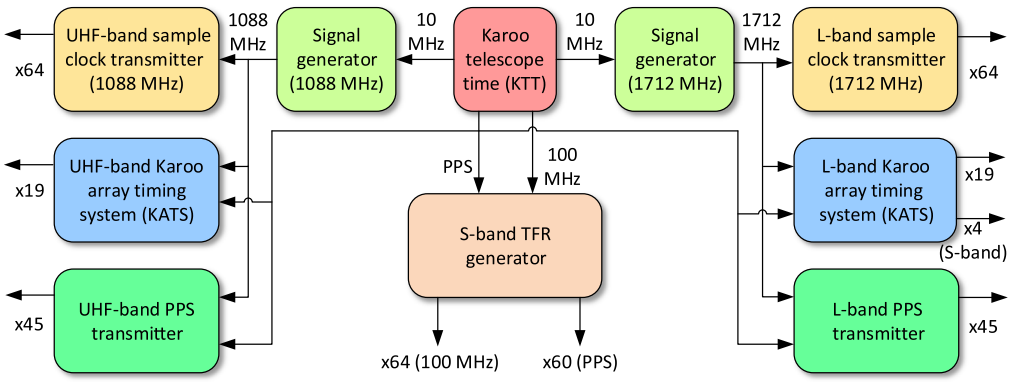

Fig. 2 The design and configuration of the reference signal distribution for the MeerKAT.

The KATS is responsible for determining timing offsets of the digitizers that are installed on the MeerKAT antennae to subnanosecond level to enable accurate timestamping of pulsars.[6] KATS is an RF-over-fiber system that operates on the principle of timing the round trip time-of-flight of a PPS-encoded RF signal. The round-trip delay is then used to determine the timing offset of a particular digitizer from the KTT. The design of the KATS has been discussed in Refs. 17, 50, and 51 where the key feature of the system is that the same laser that is used for transmission of the RF pulse is simultaneously used for measurement. The latter symmetry feature means that the system does not need specific calibration for a specific fiber. A novel reflecting directional coupler developed by Thorlabs is used to make the receiving end compact. The receiver end has a low RFI profile and is compact with low-power consumption, meaning it can be easily integrated in a digitizer.

3.5 *GNSS Tracking System Implementation*

The GNSS receivers are located inside the KDRA and connected with Eupen 5092 cable to antennas on the KDRA roof. The installation is unique in terms of measures used to prevent emissions. The antennas' DC power exits the shielded area through RFI filters from an in-house built battery-backed up DC system situated in the KDRA. Gas discharge tube lightning arrestors are used at the Leica AR25 choke-ring antennas as a precaution. There are regular occurrences of lightning in the area during the summer months.

RF emission from the KDRA is prevented by isolation amplifiers located in the GPS RF line-up after the penetration into the KDRA. Furthermore, broadband quarter-wave stubs are used in the GPS RF line-up just on the outside of the KDRA, against the shielded wall. The configuration was extensively tested in a reverberation chamber to suppress RFI levels below the requirements for MeerKAT at the KDRA. This setup was used because a "normal" configuration, as used in a metrology environment, was shown to emit significant RFI due to emissions from the geodetic time transfer receivers.

The dual-frequency Septentrio time transfer PolaRx4TR units are the primary way of measuring the time differences between GPS time and the local clocks. The receivers record data in the receiver independent exchange (RINEX)[52] format. Due to the fact that a geodetic GNSS receiver measures code pseudorange on two different carrier frequencies, a simple linear combination between two measurements provides an ionosphere-free result[53]. We convert our dual-frequency observable RINEX files to the Common GNSS Generic Time Transfer Standard[54] (CGGTTS) format, using proper antenna coordinates, antenna cable delay plus other delays to the local time scale reference point including the relatively calibrated internal hardware delay of the unit. One column of the CGGTTS files provides the offset between the local time scale and the GNSS time scale as measured from each tracked satellite for each given epoch. Time transfer between two stations can be easily computed by the common-view (CV) technique[55] after exchange of such CGGTTS files, but the available common satellite tracks depend on the distance between remote stations. It has been shown that both the GPS and the Galileo GNSS constellations can be successfully used in this method, at least if the lowest uncertainty is required.[56] The uncertainty of this technique is mostly limited by the determination of the main unit hardware delays. In the frame of the station network used for the computation of Temps Atomique International, the combined uncertainty of GNSS station relative calibrations is currently estimated at 1.7 ns for group 1 laboratories and 2.4 ns for group 2 laboratories like the SARAO, as obtained by the LNE-SYRTE from a dedicated relative calibration campaign.

We also use the newer PPP[35] for time transfer. PPP requires access to additional products from the International GNSS Service (IGS) in order to compensate for satellite ephemeris errors and satellite clock errors in the parameters of the navigation message broadcast by GNSS satellites. All GNSS data are then related to a common IGS time scale after PPP processing. The PPP technique uses the carrier phase in addition to the code of the GNSS, whereas the CV technique uses only the GNSS code signal. This allows for a better short-term stability of the measurements, thanks to the higher frequency of the GNSS carriers. PPP remains limited in uncertainty by the same station hardware delay uncertainties as CV time transfer. PPP is demonstrated for the first time on a radio telescope in this work on MeerKAT.

A secondary means of tracking the masers, and the primary means of supplying the network time, is via Spectracom GPS steered rubidium clocks. These units operate at a single-carrier frequency and is more susceptible to delays in the varying ionosphere. They are, however, more robust and generally have higher availability than the time transfer receivers and have significantly easier operational procedures, but their rubidium cells can degrade over time. They serve as the backup clocks for the whole system. They produce a PPS with an error of approximately 10 ns with respect to UTC, but the average offset is corrected in software when they are used for tracking the masers. They are also essential in detecting and correcting for possible jumps in the masers. These units serve as the PTP grandmaster clocks and Network Time Protocol servers to distribute network time to various telescope systems.

3.6 *Software Clock Tracker Implementation-VTSS*

This section describes the implementation of software to combine different clock sensors (clock combination) and smooth and correct the clock combination. This is done to produce a robust composite output that is resistant to the failure of one or more clock difference sensors or even some of the clocks. This software outputs clock tracking data for each of the four different clocks, by combining data from all of the clocks. The software is named the VTSS, which stands for the virtual time scale synthesizer.

3.6.1 *General definitions and naming conventions*

In general, there is the need to track the KTT with respect to the UTC. Up to this point, the GPS has been used as an approximation of the UTC, and this will be further evaluated in later paragraphs, as will comparisons with UTC(k) nodes in Pretoria and Paris. The KTT is defined as the time associated with the 50% amplitude of the rising edge of the PPS at the output of the KTT pulse distribution amplifier. The KTT has been measured against different external references, which are the GPS time, the UTC(ZA), and the UTC(OP). ZA refers to the South African national node for the UTC and is based in laboratory at a Pretoria (operated by the NMISA). OP refers to the French national node situated in Paris, which is operated by the LNE-SYRTE.

The resultant sets of data have been compared to each other, and the BIPM Circular T can be used to make comparisons of the KTT with respect to the UTC. In general, the KTT is estimated via a multiclock tracking mechanism that measures the KTT via CGGTTS files first with respect to GPS time. The KTT can be differenced with other the UTC(k), which has also been measured with respect to the GPS time (this was done against the NMISA). One can also measure directly with respect to GPS time. Finally, one can do comparisons to remote clocks with PPP. In the case of MeerKAT, a clock/sensor combination is done to give resiliency in KTT (for example, when a sensor fails). The internal and external "sensors" have numeric values S_i' that are related to the primary sensors S_1 through S_6 in Fig. 1. These sensors correspond to internal and external differences to other intrasystem clocks or external timescales. In practice, these sensors are TICs between all clocks, as well as four GPS receivers; two of the geodetic type and the two that are used to steer rubidium clocks.

Estimates of the KTT that can be realized by clocks $j = 1, 2, 3, 4$ (that are the two masers and the GPS steered rubidium clocks) with respect to specific references with identifiers REF (this can in practice be a number of external references) are then calculated as linear combinations (functions f_j) of S_i':

$$L_{\mathrm{REF}}^{(j)} \equiv f_j(S_i'). \tag{1}$$

Usually, a smoother, which is expressed as an operator $\tilde{S}$, can be applied to Eq. (1) to give a less noisy estimate of the KTT for the different clocks, i.e.,

$$K_{\mathrm{REF}}^{(j)} \equiv \tilde{S}\{f_j(S_i')\}. \tag{2}$$

In fact, Eq. (2) is the value usually reported in output clock files. S_i' with less variance get higher weighting in the linear combination functions f_j, subject to them being "correct."

The correctness is detected via other means, which includes internal comparisons and external comparisons to the GPS and the UTC(k). This manuscript focuses on REF = GPS but the same methodology is used for other references. In general, the sensors with respect to the GPS steered rubidium clocks get lower weighting due to their noisiness and larger difficulty in calibration (which in fact happens via the geodetic receivers). When we take into account only the geodetic receivers attached to each maser SKA1 and SKA2 (as translated to the output amplifier for the KTT) and measure these clocks via, respectively, the geodetic receivers GPS1 and GPS2 to an external reference REF, we call the unfiltered associated sensors $(\text{SKA1–REF})_M$ and $(\text{SKA2–REF})_M$. The method M refers to a specific GNSS method M like $M = \text{CV}$ or $M = \text{PPP}$ that is used for postprocessing the data. In practice, $L^{(1)}_{\text{REF}} \approx (\text{SKA1–REF})_M$ when the same method M is used for $L^{(1)}_{\text{REF}}$ (the same holds true for maser 2). Either maser SKA1 or SKA2 can be selected as the KTT (the telescope's master clock). The selection takes place via a clock selector.

3.6.2 *Tracking software implementation*

The clock tracking process is graphically illustrated in Fig. 3 and its implementation is described in this section. The tracking system uses clock combinations and smoothing to produce a *post facto* time scale that complements a real-time estimator. The real-time estimator is used to check if the system is nominal before starting high timing accuracy observations, and for preliminary timing data used in clock offset files provided to users. It is well known that lower uncertainty is obtained by employing *post facto* scales,[57] as for example, smoothers can account for data from both sides of a time interval in which a clock offset is required. The description of the KTT tracker in Ref. 16 is still relevant, although more TIC sensors are now available and used.

We initially had issues with a phase shift of the filter/smoother, however, that has now been resolved. A smoother that uses data on both sides of a produced point puts strong constraints on the value of the point versus a predictive type of filter/smoother that can be more easily perturbed and give higher uncertainty. The Savitzky–Golay filter is chosen as it does not produce a phase delay in the frequency response and therefore no unwanted time delays,[58] and is the transform $\tilde{S}$ used in practice for MeerKAT.

The compound sensors (i.e., multiple sensors for a certain clock) are weighted and summed before it is passed through a Savitzky–Golay finite impulse response (FIR) filter to form a KTT sensor, which is the offset of that clock with respect to the chosen reference. The $K^{(j)}_{\text{GPS}}$ sensors are calculated *post facto* on 9 days' worth of data, where the mid fifth day is reported to the TMC. Weighting factors, w_{ij} of contributing sensors that are summed, are the inverses of the

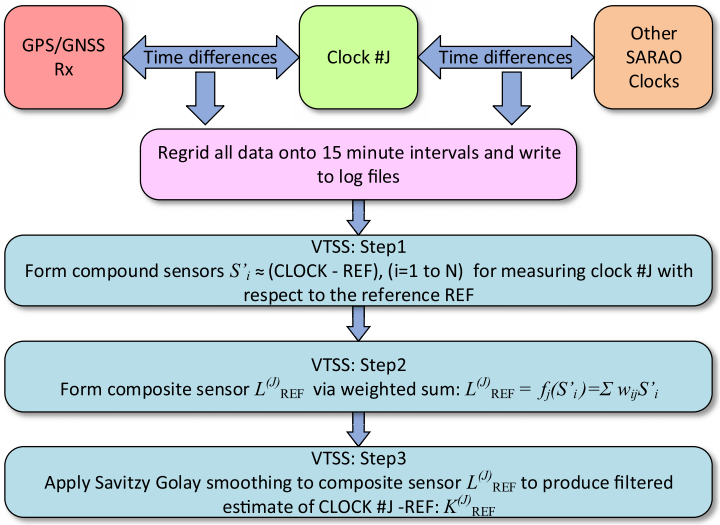

Fig. 3 The computation of KTT for clock number J, which can be one of the masers or any of the GPS steered rubidium clocks. The factors w_{ij} represent weights calculated from variances.

variances of S_i', divided by the sum of all the inverse variances of sensors contributing to $K_{\mathrm{GPS}}^{(j)}$. The implementation corrects for missing data and maser jump events are also handled. Three separate instances of all software run on three different servers to provide redundancy and robustness.

The MeerKAT masers are set to lag UTC by 150 to 450 ns for maser 1 (SKA1) and 600 to 900 ns for maser 2 (SKA2). This simplifies the monitoring system; this offset range for the masers are achieved by changing the clock's frequency divider (synthesizer) settings. TIC sensors are produced once per second, which are then averaged on 15-min intervals using a custom-built C application called REGRID. REGRID also computes an interpolation of the 16-min interval CGGTTS data from the GNSS receivers onto a 15-min grid. A 20-min tolerance on a 15-min boundary is used before the data point will be in an error state. The application also has built in missing data detection for the time interval data with a configurable acceptable tolerance for the number of missing data points before the sensor is placed into an error status. The sensors are reported to the TMC and logged to the server. The aggregated 15-min sensors are further used by the VTSS software. The VTSS software linearly combines the input sensors with calibration delay sensors to form composite sensors. In this process, sensors that are applicable to a certain clock offset with respect to the external reference are used. The ultimate reference can be GPS time or could be IGS time, etc. CV can also be performed. The tracking system's data flow is summarized in Fig. 3.

3.6.3 *Robustness, anomaly features*

There is a range of error-correcting mechanisms in the software in order to compensate for various exceptions and anomalies that occur in the clock monitoring solution; these will be discussed in a future publication. These mechanisms include the handling of missing data, sensors in an error state, and clock jumps. The software mechanism for correcting clock jumps uses the bilateral filter, which is one of a series of step detection algorithms as described in the literature.[59]

The VTSS specification also includes measures to detect the fast anomalous movement of any of the masers or geodetic receivers (four unknowns) via the other measurements by TICs (four known quantities) and is being implemented at the time of writing of this manuscript. An alarm is generated when there is a >5 ns shift in a maser in a 15 min period. This is in addition to the maser phase noise monitoring. There are several methods to detect in real time or near real time if the maser, which is selected and distributed as the KTT, is stable or not. One would know in a relatively short period if one of the time transfer receivers or a maser is malfunctioning, in order to switch the telescope time (KTT) to another maser, or replace a time transfer receiver or antenna. The resulting verified stability enables one to combine and filter the data as per the previous sections' description.

3.6.4 *Tempo2 clock files for pulsar users*

The MeerKAT clock data as produced by logging of the VTSS output are made available in a TEMPO2 compatible file format.[60] TEMPO2 is a software package that is used for the timing of pulsars. The TEMPO2 file provides the user with a file containing the KTT clock offset from the UTC over a period of $\sim$3 years. At this stage, the GPS time is used as an approximation of the UTC, as high availability is possible due to the locally produced nature of such files. There is ongoing work with both the Observatoire de Paris and the NMISA to compare the data that is produced in this way via actual KTT-UTC measurements. This is more complicated and slower partly due to the fact that the BIPM Circular T is only published once a month, and only on five daily periods. Both metrology institutes produce a real-time estimate of the UTC, with the UTC(OP) generally within 3 ns of the UTC and the UTC(ZA) within 10 ns of the UTC, as can be seen from recent BIPM Circular T bulletins. The measurement and verification of accuracy of the software tracker that is used to produce TEMPO2 files is discussed in Sec. 6 with the aid of further calculations in Appendix A. It would seem from that discussion that the low offset of the UTC(OP) from the UTC makes it a good stand-in for the UTC measurement by the

MeerKAT on intervals of 2 weeks, as the uncertainty with respect to the UTC could theoretically approach 2.1 ns when using such a processing scheme.

4 Measurements and Verification of the Clock and Time Transfer Systems

4.1 *L- and UHF-Band Qualification*

The L-band system description and qualification has already been discussed in Ref. 17. The UHF-band system has recently been installed and qualified. The design of this system is similar to that of the L-band system but operates at 1088 MHz. The system qualification consists of the measurement of the sample clock jitter and phase shift over a period of 20 min (the maximum observation interval between telescope calibrations). The phase drift of the sample clock was measured as 1.58 ps RMS after removal of the linear drift. The integrated clock jitter between 800 Hz and 1 MHz was measured as 67 fs.

4.2 *KATS Qualification and Measurements*

4.2.1 *End-to-end measurements on KATS's offset and temperature sensitivity*

The KATS system was qualified by connecting a TIC to the output of a digitizer that is being measured by the KATS. This allows measurement of the actual time offset from the KTT and verification of the offsets measured by the KATS using various lengths of fiber. The KATS units were tested over their operational temperature range of the KDRA. The results are plotted in Fig. 4. The results show that the KATS has a bias of <0.15 ns. More importantly, the results also show that the accuracy of the UHF-band KATS system is <0.5 ns at every measurement point and therefore meets the required 1.6 ns specification of MeerKAT. The low uncertainty of KATS has been instrumental in achieving overall low uncertainty on the data streams that are generated at the digitizers.

4.2.2 *Seasonal measurements*

The KATS results show that it has been correcting seasonally induced drift, and which is well understood as can be seen from Fig. 5. The site time-delay data were fitted using ground diffusivity that were measured by knowing site temperatures and/or phase shifts that are apparent from measured site temperatures and delay changes. This system has, therefore, been shown to behave predictably over seasons.

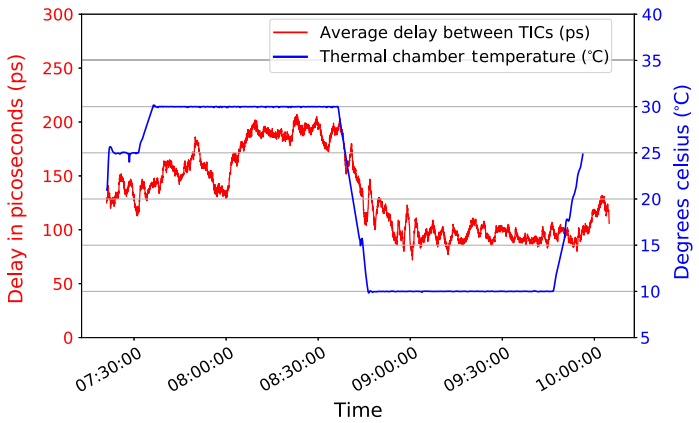

Fig. 4 The results of the UHF-band KATS temperature qualification. The blue trace is the chamber temperature, and the red trace is the difference between the measured KATS offset and the actual delay to the digitizer.

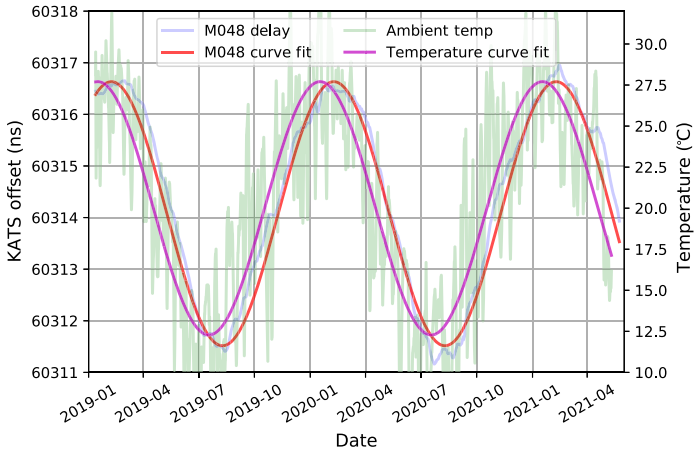

Fig. 5 Measured variation for the round-trip delay via the KATS data to the digitizer on antenna M048. This antenna is situated at 12 km from the KDRA. The weather station temperature data are also shown for comparison. Sinusoids have been fitted to the data to determine the phase shift between the weather data and the measured cable delays.

4.2.3 *Discussion of absolute time transfer via KATS*

The KATS system has also been deployed to the UHF-band digitizers on the same antennae as used by the L-band system. The delays compare well with those of the L-band measurement, although there are small fiber length differences due to fiber cable routing differences on each antenna. The L- and UHF-band system makes use of different RF filters in their recovery circuits, and there are calibrated delays that are different due to these different filters. It does not make a difference though in the measured delay via the KATS as the detection and measurement sides are symmetric. The measurements do show that the operation of the KATS system is well understood and repeatable and stable over years. The accuracy of the KATS time delay and compensation is evaluated as to be <0.5 ns. Further verification of the time transfer system from the clocks to digitizers happened via comparing the KATS compensated timing to different antennas to the fringe correlation derived timing, as calculated via the telescope's correlator–beamformer and science data processor systems.

5 Basic Measurements and Verification of the Clock Tracker

5.1 *Basic Measurement and Verification and Reduction of Variance by Smoother*

An extensive set of verifications has been done on the tracking system and will be described in more detail in further publication, but the outline of what was done is given here. The basic operation of the VTSS clock tracker is checked via measurement against GPS steered rubidium clocks, measurements of offsets and calibration of the other receivers as is described in the next section. All the underlying weighted sensors making up $L_{\mathrm{REF}}^{(j)}$ are measured against each other for individual alignment, and the GPS steered rubidium clock sensors are aligned to other data using two-week-long integration. External comparison has also been done using time transfer. The smoothing was verified to give numerical numbers that reduced the clock combinations' ($L_{\mathrm{REF}}^{(j)}$'s) noise, and the correct operation of the clock tracker when the maser synthesizer frequency is changed was also verified. These two types of measurements are discussed below. In all cases, the reference for checking measurements is the time transfer receivers that are directly connected to the masers, aided by a TIC connected between the masers.

The trackers could be used after a number of self-consistency checks and telescope level checks, balances, and tests. This paragraph shows some subsequent measurement results. Figure 6 depicts $L_{\mathrm{GPS}}^{(1)}$ over a 7-day period, before and after the FIR smoother filter is applied ($L_{\mathrm{GPS}}^{(1)}$ becomes $K_{\mathrm{GPS}}^{(1)}$ after application of the filter). Before the FIR smoother is applied the

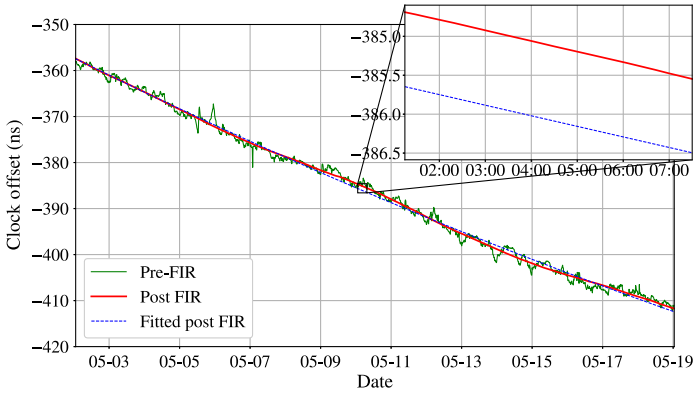

Fig. 6 The maser 1 clock offset as tracked by the VTSS during a part of May 2021. The green line represents the clock combination $L^{(1)}_{\mathrm{GPS}}$, and the red line is $K^{(1)}_{\mathrm{GPS}}$. The blue line is a parabolic fit to $L^{(1)}_{\mathrm{GPS}}$, the inset shows a magnified part of the curve.

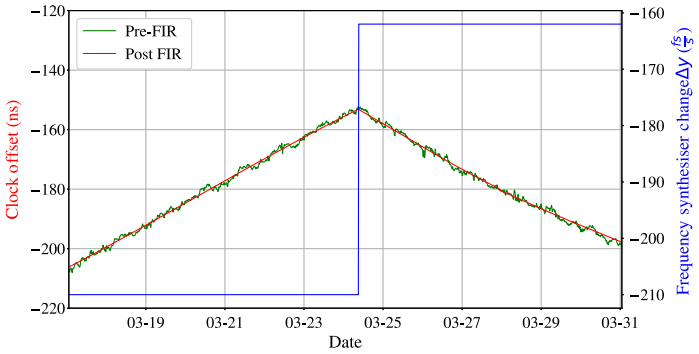

Fig. 7 The smooth and reliable operation of the VTSS over a synthesizer change induced by software commands. The green line shows the unfiltered data $L^{(1)}_{\mathrm{GPS}}$. The Savitzky–Golay filter is able to operate with the discontinuity (the sharp change in offset) as the synthesizer change is synthetically removed from the data so that the filter can operate on a smoothly evolving signal, which corresponds to the underlying microwave cavity of the maser. This synthesizer change is then synthetically added back, and the red filtered line is then clearly a well filtered version of the unfiltered clock combined data. The blue line shows the change in the frequency synthesizer settings.

standard deviation of the clock offset data is 1.09 ns, this decreases to 0.38 ns after the FIR smoother is applied. Figure 7 shows the filtered and unfiltered clock offset data as well as the change in frequency synthesizer settings for maser 1 over a steering event, which occurred on March 24, 2021 at 07:00 am UTC. The latter results illustrates that the software tracker works smoothly and with high accuracy over discontinuous operational events that are routinely encountered. Further measurements, calculations, and analysis relating to the accuracy of the VTSS clock tracker and therefore the overall TFR system timing uncertainty are described in Sec. 6.

5.2 *Measurement of Uncertainty of Software Jump Corrector*

Numerical tests verified that it was possible to detect and measure jumps up to a size of 100 ns with a magnitude error of <300 ps with a standard deviation of ≤120 ps. This mechanism was not activated after the hardware correction of the ESD but would be useful if the maser is disturbed in some other way, when personnel are working there. More detail will be given in a further publication on the specialized software for the TFR.

6 Measurements and Verification Related to Timing Accuracy

6.1 *Measurement and Evaluation of Geodetic Time Transfer GNSS System Antenna Mount and Receiver Chain Stability*

The geodetic GNSS time transfer system was characterized via measurement for positional and drift stability over many years. The position changes were first measured and correlated with other measurements on the subcontinent. The position of the antennas can be carefully tracked via PPP. The position in space of the antenna phase centers has been calculated between August 2019 and February 2021. We have determined that GPS1 and GPS2 moved by an amount of 38.3 and 39.1 mm, respectively, in a north-easterly direction over a period of ~18 months. This equates to a shift of ~26.5 mm per year in a north-easterly direction that matches the continental drift of similar stations in South Africa quite well.[61] For example, the drift in the Sutherland and the HartRAO stations are 25.3 and 25.4 mm per year, respectively[62] (using the Jet Propulsion Laboratory values). Therefore, the antenna bases have good stability, and the motion is dominated not by building movement but by continental shelf movement. This would seem to indicate that the antenna mounts are indeed close to geodetic quality. In fact, the phase center of the MeerKAT was determined with respect to the antennas.

Some further stability characterization of the GNSS time transfer receivers consisted of measuring the differences between the masers as through receiving signals via the GPS. These latter maser difference measurements via the GPS signals and the geodetic receivers were compared to a much more stable measurement of the time differences between the same two masers as performed via the TIC connected in between the same two clocks. We further studied the statistics of the difference between the GPS and TIC measurements (a double difference) between the same two masers. We calculated the modified Allan deviation as $\leq 3 \times 10^{-17}$ above 10^5 s and also the time deviation (TDEV) of this double differences (the latter is shown in Fig. 8). Just a single calibration was assumed to be able to only look at the drift. It is clear that there is instability in PPP and geodetic timing increasing with time, which results in an unbounded characteristic in the timing deviation. This does mean calibration does have to be periodically performed as further discussed in the rest of this paper. One cannot take a single calibration and assume that will be sufficient for the rest of the telescope lifetime. Of course, common effects that might have occurred would not have shown up in the differences of GPS1 and GPS2, so their absolute drift could have been bigger, than only the differences between them could suggest.

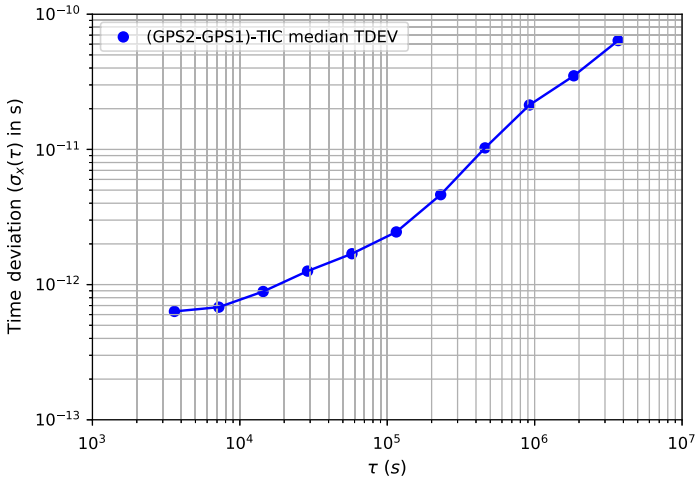

Fig. 8 The TDEV of the measured differences between the time transfer receivers via GPS CV time transfer. This graph is representative of timing shifts that are due to difference mode effects as a function of observation time τ. TIC refers to the time interval counter connected between the two masers. The masers are measured against external references through the two time transfer receivers GPS1 and GPS2.

In MeerKAT's lifetime there have been two calibrations happening: one via the NMISA and one via the LNE-SYRTE. In 2021, this resulted in a step of 1.54 ns applied to the timing, when the newer calibration was used, in the tracking of the KTT described in the next paragraph.

6.1.1 *Discussion of GNSS receiver and antenna mount drift measurements*

The positional and drift stability of the GNSS time transfer system corresponds to the subcontinent's drift and an estimated drift rate of the GNSS receivers' timing bias of <1 ns peak to peak over 2 years, respectively. Of course, drift can be quickly degraded for any of the time transfer receivers or their antennas. The latter means that the system has to be periodically recalibrated, and means for doing such regularly is developed through an optically isolated calibrator, so as to continuously keep the uncertainty related to the time transfer receivers low. The GNSS system calibration is further discussed in the next section.

6.2 *GNSS Receiver Calibration*

The PolaRx4TR units have internal delays that are calibrated using a relative calibration method that is quite similar to that as specified by the BIPM,[63,64] except that the traveling receiver has been supplied by the SARAO. Measurement closure has to some degree being checked via measurement against more than one metrology institute and not sending the receiver back to the same institute. Furthermore, constants are measured to align the PPS from the GPS steered rubidium clocks' average's to UTC. The weighting factors are summarized in a clock configuration file that is applied by the VTSS software to compute $K_{\mathrm{GPS}}^{(j)}$. Further details on TFR timing uncertainty, which mainly derives from the GNSS receivers, are given in Appendix A. Cable delays and uncertainties related to measurements of delays are discussed in the next section, as it is handled separately to properly account for system delays and uncertainties.

6.3 *Delay Measurement*

The timing latching points in the Septentrio time transfer receivers are related to the PPS edge at the output of the KTT distribution amplifier via cable and delay measurements and the uncertainty of such. We have measured the delays with multiple types of test equipment. We also calculated systematics, which are dominated by cable dispersion and filtering effects and instrumentation filtering together with trigger level interaction[65] and which were first quantitatively dealt with by researchers at the LNE-SYRTE.[66] Our internal measurement methods were compared by the singular value decomposition (SVD).[67,68] The SVD is related to the principal component analysis.[69,70]

The measurements for the comparisons are corrected for delays in connectors, as well as simulated corrections based on measured cable parameters, in order to transform the data into equivalent 50% triggered TIC time delays. One can obtain root-mean-square deviations (RMSD) for each method from a global SVD fit over the 1.5- to 25-m cable range as is shown in Table 2. The fit was adjusted to go through the origin before the RMSD evaluation. Such an evaluation

Table 2 RMSD from a SVD determined line fit for a Guidetech TIC, Anritsu VNA measuring group delay and $|S_{21}|$ (the amplitude of transmission) and a Rhode and Schwarz (R&S) VNA doing a time domain measurement via a built-in inverse Fourier transform function. The VNA measurements were processed to give TIC equivalent measurements, as in reality, a TIC measured delay is not the same as the group delay measurement or the time domain inverse of a complex S_{21} measurement (the *S*-parameter corresponding to the complex transmission coefficient).

RMSD of the Guidetech TIC via time delay (ps)	82.3
RMSD of Anritsu VNA via group delay (ps)	38.3
RMSD of the time delay R&S VNA used time domain mode (ps)	45.34

gives a measurable idea at the SARAO of likely deviation or possible systematic deviation from an ideal measurement, if it assumed that the all measurements together give a better idea of the "correct/true" measurement of the cable. Another type of TIC was compared with the first time interval counter that were tested against the VNA's as well, as different TICs are used in practice on site. There is an attempt to further understand differences between the methods, and a further in-depth analysis of uncertainties associated with these specific apparatus and methods are being undertaken. The VNA group delay measurements are used for the GNSS RF P_1 and P_2-delays in the cables between the GNSS antennas and the geodetic receivers, and the TIC measurements typically in the cables that transport PPS signals.

For the TIC, some measurements were numerically compensated to correct for dispersion and the trigger level effects. The TIC skew can be compensated for and measured by doing the measurement in "reverse." This is done via interchangeably switching start and stop ports via physically swapping the two signal cables and furthermore by changing the instrumentation setting between the two measurement ports (the normal start channel becomes the stop channel and vice versa). We chose to adopt a conservative systematic uncertainty of 200 ps (one standard deviation) for all cable measurement, as is based on the analysis and uncertainty proposed by Keysight electronics.[71]

The impact that the trigger level of the GNSS receiver has on the system was investigated for completeness' sake. The cables from the maser are measured in a differential way: a set of cables go to the geodetic GNSS receivers, and the different sets go to the PDAs as can be seen from Fig. 9. The Septentrio receivers have complementary metal semiconductor (CMOS) gates with a 10-kΩ pulldown resistor and triggers in a dynamic sense at a value determined by their threshold voltage and/or transistor characteristics.[72–74] The latter switching characteristics depends on among other things on the relative physical sizes and microarchitecture of the positive-channel

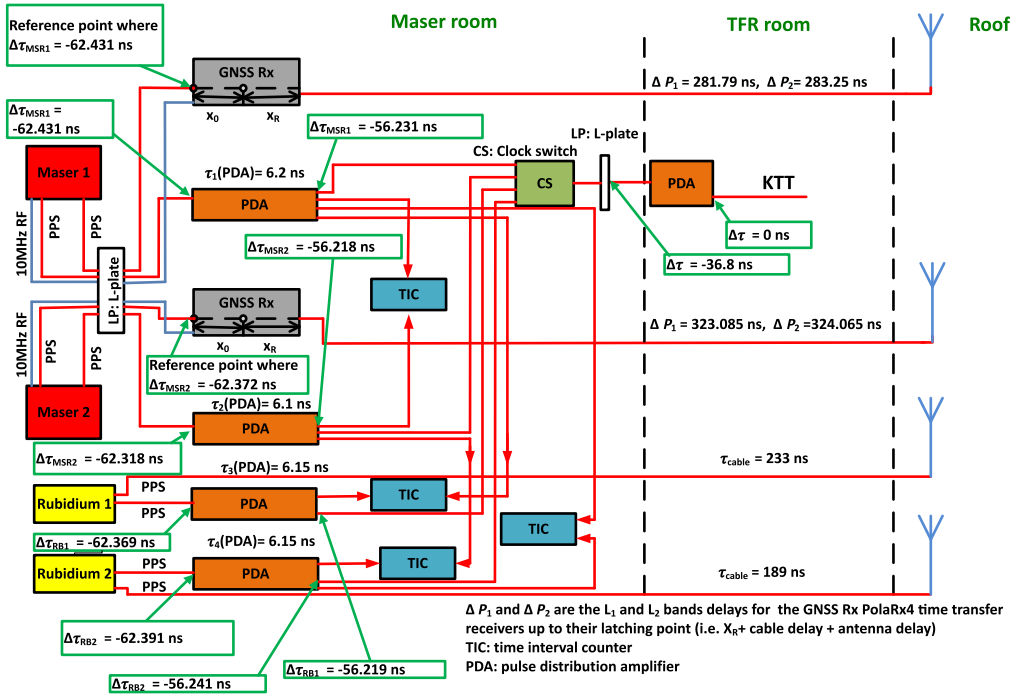

Fig. 9 Some of the delays in the clock system with respect to the KTT reference. The KTT's physical location corresponds to the back panel of a pulse distribution amplifier where the relative delay $\Delta\tau$ is defined to be zero. The KTT may be realized by the four clocks connected to the output pulse distribution amplifier via a clock switch. The backward delays $\Delta\tau_{CLCK}$ (where CLCK is an abbreviation for a clock) is shown in the diagram. Rubidium 1 and rubidium 2 are GPS steered rubidium clocks with different cable lengths with delays of τ_{CABLE} to the roof antennas as indicated.

and negative-channel metal oxide transistors that together make up CMOS.[72,75] The PDA for a maser triggers at 1.5 V. It is assumed that the Septentrio that is also connected to the maser with a very similar length cable also has a nominal 1.5 V trigger voltage similar to Renesas logic.[76] The actual designed voltage could not be found from the manufacturer, and it is assumed that the threshold voltage is 1.5 ± 0.3 V for 3.3 V CMOS as used in the receiver. (Many times CMOS is designed to trigger at 50% of the supply.) The delay changes due to this possible range of trigger values are ∼100 ps when simulated with extracted parameters for the input pulse as found in the setup. In general, there is, therefore, differential delay between these three sets of apparatus (GNSS receiver, PDA, and TIC) that is used in deployment or delay measurement and when connected to the same signal. But in our case, the internal delay measurement on a TIC (there is always a TIC connected on site to measure internal delay on the GNSS receivers continuously) is affected in the same but opposite way than the effective external cable delay as determined by the trigger level of the GNSS receiver. The simultaneous GNSS and TIC measurements mean that there is no contribution of uncertainty in trigger level of the GNSS receiver to the first order, to the total system delay uncertainty.

The skew of the PDA is also taken into account for total uncertainty estimation, as the relative delay of each port with respect to a reference port has not been measured. On a different point, we looked at corrections to delay measurements due to cable dispersion, pulse shapes, and detection bandwidths, and the modeling could reproduce pulse shapes on cables, and such corrections are conservatively assumed to have an uncertainty of 50 ps. For comparison, the largest modeled correction to correctly account for delay is 144 ps. In the end, all uncertainties are summarized in Table 3 in Appendix A. It should be noted that delays and effects related to the Septentrio receiver is accounted for by the number with magnitude $u_{b,31} = 0.29$ ns in Table 3. There is also separate accounting for the uncertainty in the delay measurements from the maser to the output PDA (where KTT is defined) via the number $u_{b,32} = 0.37$ ns. There is also uncertainty contributed by the setup of the travelling receiver (in measured delays from the maser clock output to the receiver's latching point). This is described by a component with the magnitude $u_{b,21} = 0.29$ ns. Finally, there is an uncertainty contribution due to uncertainty in the measurement of the GPS cable with the magnitude $u_{b,41} = 0.2$ ns that is used with the travelling calibrator. When taking all cable and measurement uncertainties into account the timing at the KTT output amplifier is found to have a combined uncertainty of 4.1 ns.

6.4 *Comparison with External Timescales*

6.4.1 *Comparisons with the National Metrology Institute of South Africa*

Initial comparisons between $K_{\mathrm{GPS}}^{(1)}$ and KTT-UTC (as measured via CV with the NMISA) were done in 2020 as shown in Fig. 10, which were used in an initial evaluation of uncertainty that is revised in a more formal way in Sec. 6.5. A quadratic trend was removed from data to do the comparison. The blue line in Fig. 10 shows that time scale steers can be clearly seen when comparing to the UTC(ZA) at the NMISA via the GPS CV method. The measurements were compared on a relatively fine grid, and the Circular T had to be interpolated by splines to do the corrections from the UTC(ZA) to the UTC. It was found that the KTT, when differenced with the local (Losberg) received GPS time (in the $K_{\mathrm{GPS}}^{(1)}$-form), did not exhibit a large RMS difference to the UTC (the red curve) at the time. The dark green trace illustrated the futility in using Circular T corrections for the direct KTT to GPS time data (in the $K_{\mathrm{GPS}}^{(1)}$-form), and therefore this was also discouraged among users. It needs to be noted that the Savitzky–Golay filter used a computational window of 48 h last year (2020), which was increased to 9 days (216 h), after it was found that the masers are very stable. These longer filters still represent clock differences well, but reduce noise on short observation periods. Measurements show that the Allan deviation on the DMTD analyzer connected between the masers can approach 2×10^{-16} at times, depending on the settings of the maser synthesizers/frequency dividers. It is shown in Appendix A how the evaluation and analysis of data as is shown in Fig. 10 was pointing to the standard deviation of the KTT (therefore its uncertainty) of ∼5 ns.

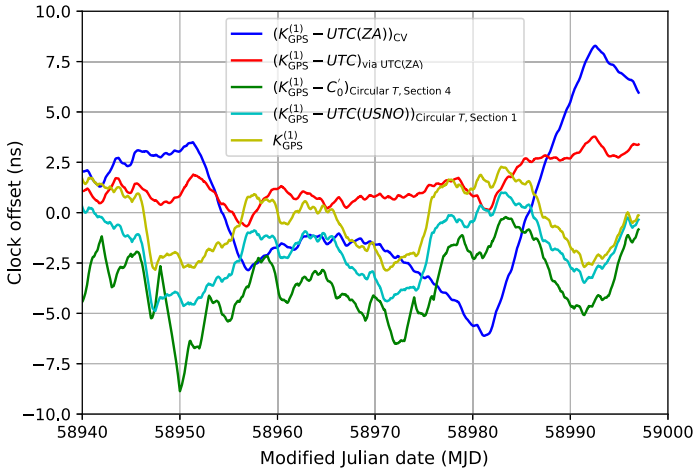

Fig. 10 The offset of the KTT is computed through various methods are shown. A quadratic fit is removed. The yellow trace is the KTT clock offsets from the GPS time (CGGTTS). The blue trace is the CV offset of the KTT from the UTC(ZA) with maser steering clearly visible in these results. The red trace shows the KTT clock offset by correcting the blue curve with spline interpolated BIPM Circular T data for the UTC(ZA). The green trace is the offset from the UTC(USNO) by correcting the KTT—GPS time offsets with the GPS corrections in section 4 of the BIPM Circular T. The cyan trace is the offset of the KTT from the UTC by applying spline interpolated UTC-UTC(USNO) data as published in section 1 of the BIPM Circular T.

6.4.2 *Calibration against OP reference station, measurements with the LNE-SYRTE and PPP transfer with the UTC(OP)*

After a relative calibration of one SARAO GNSS station by LNE-SYRTE against the OP reference station OP71 in late 2020, the resulting hardware delays were used to relatively calibrate other fixed SARAO GNSS stations. Different time transfer techniques were then applied between SKA1 (maser 1 via geodetic receiver GPS1) and SKA2 (maser 2 via geodetic receiver GPS2) on one side, and the references UTC(ZA), UTC(OP), UTC(USNO), and the GPS time on the other side. The most simple GNSS time transfer technique is CV between stations, which is commonly achieved between the SARAO and the NMISA, and was used in the previous section. Due to the MeerKAT's location, there is only a low number of GPS satellites in CV with the OP (and sometimes none), which leads to large noise and fluctuations in the CV[55,77,78] results. Therefore, time transfer based on the PPP processing developed by the National Resource Canada (NRCan)[35] was used. This PPP difference was computed between SKA1 and SKA2, and the UTC(OP), which is the realization of the UTC built by the LNE-SYRTE, based on a set of hydrogen masers steered daily in frequency by cesium and rubidium fountains operated at the OP, and on the UTC monthly after publication of the BIPM Circular T.[79] Over the last few years, the departure of the UTC(OP) from the UTC stayed within 2 ns almost over all of the time, as can be seen in the BIPM Circular T. Thanks to the use of the carriers in addition to the code of the GPS signal, the noise of PPP time transfer stays largely below 1 ns.

The offsets of the KTT (in the forms of SKA1 and SKA2), and the UTC(OP) were measured via the GNSS geodetic receivers via local clock differences of both the KTT at Losberg (site of the MeerKAT) to the GPS time and the UTC(OP) Paris to the GPS time as received on these different sites via the specific satellites that each station has in view. This was done using the RINEX to CGGTTS conversion software[54] (called R2CGGTTS) and this was executed both for the KTT and the UTC(OP) and such results compared to find the clock differences between the KTT (in the forms of SKA1 and SKA2) and the UTC(OP). The difference between the KTT and the UTC(OP) can also be determined by calculating the offset of each station from the IGS rapid timescale, through processing RINEX files with satellite ephemeris and clock corrections as distributed by the IGS using the rapid data products.[35–37] The PPP process provides, amongst others, the clock offset of SKA1 and the UTC(OP) from the IGS rapid timescale. By subtracting these data sets from each other, the clock offset between SKA1 and the UTC(OP) can be

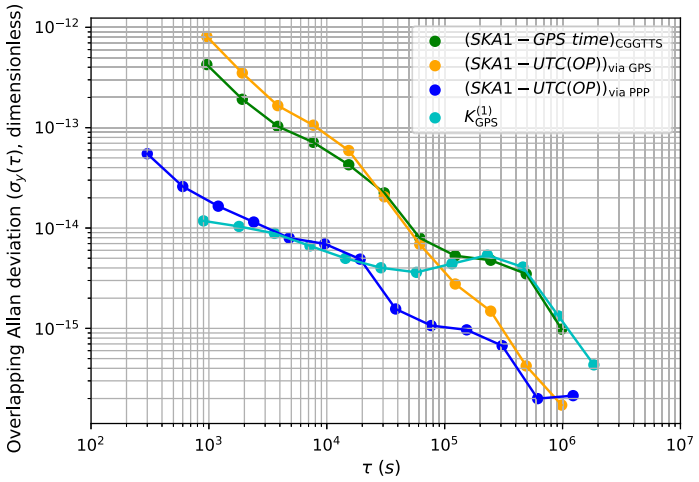

Fig. 11 The overlapping Allan deviation of the phase residuals for different differences from a polynomial trend. The stability of $K^{(1)}_{GPS}$ follows that of the PPP trace between 100 and 20,000 s due to the filtering/smoothing of the data set. However, over timescales >20,000 s, it follows the stability of the GPS time.

calculated. In addition, the computation has been corrected using the P_3 combination of the hardware delays for both stations. The phase residuals were calculated by subtracting a quadratic fit from the clock data over the period from MJD 59300 and the results further analyzed using the Overlapping Allan Deviation (OADEV) method[80] as shown in Fig. 11. The result for SKA2 is very similar showing consistency in tracking for both masers. The difference between SKA1 and the UTC can be estimated by measuring the difference between SKA1 and the UTC(OP) via PPP and also knowing the differences between the UTC and the UTC(OP) via the Circular T, thereby enabling one to estimate a difference SKA1–UTC.

The RMS differences between the SKA1–UTC data and $K^{(1)}_{GPS}$ can be calculated by decimating $K^{(1)}_{GPS}$ data onto a 5-day grid. The RMS difference between $K^{(1)}_{GPS}$ and SKA1–UTC was measured as 2 ns RMS and the difference between SKA1–UTC(OP) (via the PPP method) and SKA1–UTC was measured as 293 ps over a 2-month period. The $K^{(1)}_{GPS}$ reduces fast fluctuations (with respect to direct to GPS time observations) as can be seen from Fig. 11. Due to the 9-day window of the Savitzky–Golay filter, the OADEV does not improve beyond 2×10^5 s. It can be seen that it could be beneficial to lengthen the smoothing filter out to 10^6 s, which would reduce the fluctuations in the clock file due to the GPS's instability. This would, however, disallow the publishing of a bi-weekly clock file with these results and for that scenario a more stable and accurate predictor like the UCT(OP) is useful. If one could wait for an entire month, the UTC(ZA) would be better than the GPS time, as the BIPM Circular T could have been applied to the comparisons between $K^{(1)}_{GPS}$ and UTC(ZA) to get a low-uncertainty estimate of the KTT offset. It can also be seen from Fig. 11 that the noise of PPP is much lower than that of the other methods.

Figure 11 indicates the good relative stability between SKA1 and the UTC(OP). Similar stability is known to exist for SKA2 due to the in-house comparison via the DMTD connected between SKA1 and SKA2.

The time transfer methods and stability of the receivers were measured and tested to some degree by CV and PPP differences between the GPS1 and GPS2, which are connected to SKA1 and SKA2, respectively. These measurements are useful since SKA1 and SKA2 are also connected to a TIC that records the offset between the PPS signals of the clocks. This TIC data can be used to calculate the double difference. This is done by first calculating $(\text{SKA2–SKA1})|_{\text{PPP}} = (\text{SKA2–IGS}_R)\text{–}(\text{SKA1–IGS}_R)$, where IGS_R refers to the IGS timescale offset. The double difference is defined and calculated as $(\text{SKA2–SKA1})|_{\text{TIC}} - (\text{SKA2–SKA1})|_{\text{PPP}}$. Similarly, the double difference can also be calculated using the CV data between the two SARAO stations: $(\text{SKA2–SKA1})|_{\text{TIC}} - (\text{SKA2–SKA1})|_{\text{CV}}$. These comparisons show $\lesssim$500 ps difference between TIC measurements and PPP calculated clock differences

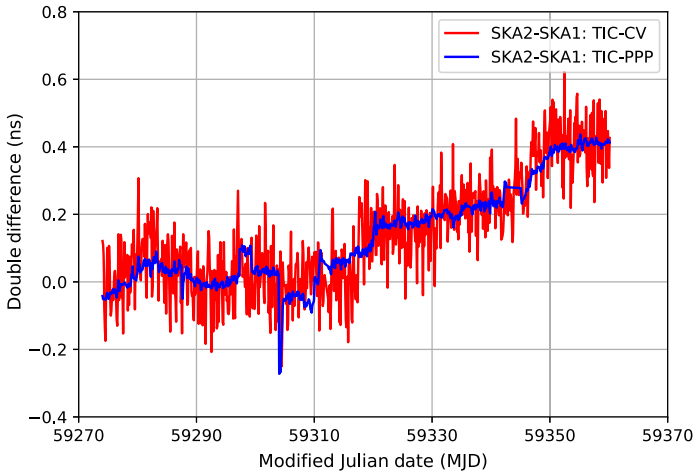

Fig. 12 Double differences calculated by subtracting the SKA2 to SKA1 offset, calculated through CV, from the TIC data. This difference is shown in red. Similarly, the SKA2 to SKA1 offset, calculated through PPP with UTC(OP), and differenced with the TIC data is shown in blue.

as shown in Fig. 12. This is a very useful internal consistency check as well as further evidence of the stability of the time transfer methods that are utilized.

6.5 *Evaluation of Tracking Uncertainty*

6.5.1 *Uncertainty of the GPS time with respect to the UTC*

The MeerKAT has been using the GPS as a reference due to its high availability, and an assessment of the KTT to the UTC uncertainty is needed when doing such a type of monitoring. This is a reasonable approximation as the United States Naval Observatory (USNO) steers the GPS time to the UTC(USNO) and uses a large number of atomic clocks to reach high stability[81] and it therefore has a good prediction capability of the UTC. The properties of the GPS time were analyzed based on results from the Circular T and published data from the USNO.[82]

It can be observed that there are two ways to determine UTC-GPS Time. The USNO publishes the differences between UTC(USNO)-GPS time, as for example, can be seen in a graph in Ref. 81. Then UTC-GPS time can be inferred by subtracting UTC(USNO)-GPS time from the UTC-UTC(USNO) data that is published in section 1 of the BIPM Circular T. The value of UTC-UTC(USNO) as distributed by the BIPM is also published in section 4 of the Circular T. The daily values $C_0' = \text{UTC} - \text{UTC(USNO)}_{\text{GPS}} = \text{UTC} - \text{broadcast GPS time}$ (section 4 of Circular T) is currently calculated using data from one of the SYRTE receivers (OP71 or OPM6), but it is based on L_1 C/A (course acquisition) only, not an ionospheric free P_3. Thus it is more noisy, because the ionospheric delay is based on a model and not subtracted by the P_3 combination. The receiver C_1 delay has been calibrated during a group 1 BIPM relative calibration campaign.

The data from a USNO plot of GPS time-UTC(USNO)[82] were digitized from the graph in the publication[81] and the Circular T section 1 and were used to subtract UTC–UTC(USNO) to obtain a graph for GPS time-UTC, which were compared over the timespan encompassing ~57,400 to ~58,600 MJD. The comparative timing deviations are shown in Fig. 13. The TDEV for the USNO (digitized) data is seemingly unphysically small for $\tau \leq 10$ days, likely due to the method of digitization, and spline interpolation to obtain the values at small intervals from the graph in Ref. 82. It does seem that the BIPM data are more correct for $\tau \leq 10$ days at least in the presented graph. The two curves in Fig. 13 seem to follow similar trends up to about 200 days, with the BIPM only data being more noisy. The USNO monitoring of GPS time-UTC(USNO) seems to suggest that in fact both the UTC(USNO) and the GPS time, which is steered to the latter, converge to the UTC as the red curve becomes <0.1 ns for long averaging times. This would agree with the mission of the USNO to steer the UTC(USNO) towards UTC and to steer the GPS time in turn to the UTC(USNO). Nevertheless, the system needs to be independently measured by the

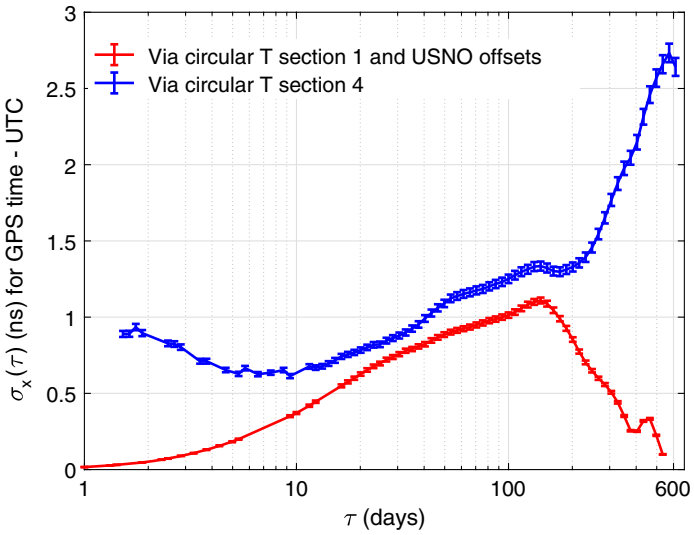

Fig. 13 Red: the TDEV of the GPS time minus the UTC as a function of the observation time τ obtained via graph digitized USNO data combined with spline interpolation of the Circular T's publication of UTC-UTC(USNO), and in blue, the TDEV as obtained by processing the raw data from the Circular T's section 4.

BIPM. The resultant blue curve as obtained by simply using the Circular T also seems to reach a plateau at nearly 600 days of <2.7 ns—this could be related to calibration intervals. The peak/plateau of the blue curve is used as the standard deviation of GPS time-UTC for the sake of uncertainty calculations.

6.5.2 *Calibration uncertainty: receiver and delays*

The link to the UTC via the GPS time is one of the timing uncertainty contributors, and the other larger part comes from the GNSS receivers themselves. The fused KTT to reference offset sensor has an absolute time delay/offset uncertainty that are determined by the offset uncertainty of the different underlying sensors, which are all dominated by the type B uncertainty for the GNSS time transfer receivers, which are all calibrated from a single traveling time transfer receiver that was shipped to the Observatoire de Paris and the NMISA. One finds that the addition and fusing of sensors does not remove this offset in the fused sensor, due to correlation in the offset of the sensors.[83,84] In the worst case, one has to assume a measurement uncertainty of 4.0 ns in the calibration (and this is one reason absolute calibration is being pursued). As shown in Appendix A, there is little contribution to uncertainty due to the uncertainty in measurement of cable delays, and even when such is accounted for one gets a total uncertainty figure of $u_{\mathrm{CAL}} = 4.1$ ns.

6.5.3 *Combined uncertainty*

The other uncertainty contributor is noise fluctuations of $K_{\mathrm{GPS}}^{(j)}$ that are left over after the smoothing and is determined as the RMS difference between a polynomial fit to the maser offset over a long period and the output of the smoother. It was previously indicated that this is 0.4 ns. The combined uncertainty then takes into account this measurement noise fluctuation, the uncertainty of tracking with respect to UTC when using GPS, and the calibration delay uncertainties of the system that includes the time transfer receivers. Therefore, the combined uncertainty can be calculated by adding these three components in quadrature. This means the combined uncertainty of the KTT with respect to the UTC, when using the GPS time for such tracking is $\sqrt{4.1^2 + 2.7^2 + 0.4^2} = 4.925$ ns. This is very similar to the amounts as calculated in Appendix A.1 when estimates were first done based on the comparisons with the NMISA. As is shown in Appendix A, one can achieve substantially smaller uncertainty when measuring against a group 1 laboratory like the SYRTE/Observatoire Paris, and when doing absolute calibration, even when bi-weekly timing reports are done, as with the MeerKAT.

7 Ongoing Work for MeerKAT and MeerKAT Extension Telescopes

There is ongoing work on parts of the MeerKAT TFR that are part of the original requirements and associated product breakdown structure. This includes work on data integrity and redundancy via hardware and software, a specially built calibrator that is optically isolated from the building and the addition of a specially built stabilized crystal (similar to the maser crystals) for three cornered hat monitoring[85] of the masers on short-time spans. Furthermore, the measurements with respect to the OP show that PPP is a feasible method of time transfer, and it could be beneficial to do predictions into the present of such data. This is considered, when one wants to try and synthesize a clock with a certain specific offset in the present, which is useful in measurement purposes. The work in this domain is done by using PPP code developed by different institutions, and where execution of such code is scripted to run automatically. The examples used in this publication used NRCAN, but we have access to at least two other packages, and comparisons will be done between these packages. Furthermore, there are several efforts to enable real-time PPP time transfer.[86–90] The SARAO also has an absolutely calibrated simulator[91–93] with specialized antennas and is in the process of setting up a measurement chamber with radio absorbing material to obtain very low and often repeatable measurement and calibration on any time transfer receiver or the optically isolated receiver as mentioned above.

8 Discussion and Conclusion

Mature commercial off the shelf technology with some custom developed systems (where no commercial products existed) was utilized to achieve the MeerKAT system requirements. The implementation was requirements driven and verified or qualified via measurement and/or analysis as appropriate at every stage in a systems engineering-based approach closely related to ISO/IEC 15288.[94] A mature network technology in the form of the PTP was used that can propagate over the normal Ethernet network and also control the antennas. It has furthermore been demonstrated that it is possible to reliably operate masers in a commercial fluid heated/cooled box in cascade with specialized laboratory type air conditioners in a greater data rack area where there are substantial environmental change over a day or other time periods as certain computing loads switch on or off. The measured stability of the masers shows that the ± 0.2°C temperature regulation works well. This level of performance would not have been able without the usage of the heater cooler boxes, due to the temperature fluctuation of ± 2°C that are seen in the maser room, due to computing heat loads being activated and stopped in the KDRA. This also means that should any atomic clocks be added in the future to the maser room that they also need to have similar stringent temperature controls as masers can have a dynamic frequency change of -4×10^{-14} for a 2°C temperature step change.[95] Static temperature effects are still appreciable according to the same literature ($\sim -3.4 \times 10^{-15}$°C^{-1}). Literature shows that it is important to screen the masers from magnetic fields, and the SARAO installation also has taken care in putting shields around DC supply lines, apart from the built-in μ-metal shields in the masers.

The accurate propagation and measurement of the PPS was challenging, as no methods existed to make this possible, through only two possible interfaces namely analog fiber signals and a 10-Gb/s data interface and where only fractional Watt power dissipation was allowed. The PPS and KATS time propagation systems were developed, and the digitizer design updated to enable nanosecond level registration of time via novel mechanisms. On a telescope systems level, special time management software was written as it was clear not a single heralded time could be used in a distributed system like a radio interferometer. The practical situation of heralding the exact UTC in real time is impossible as the UTC is a *post facto* timescale and as any transmission of time by any known protocol and method comes with inherent error and uncertainty. No two points that are physically separated can via any method be perfectly connected in a time sense, as correcting for time delay boils down to a measurement problem for the actual delay or difference, and measurement have uncertainty and noise associated with it. There is a demonstrated need to measure and compare multiple points in a subarray to give a time-tag to that subarray, as a single measurement by itself does not have statistical significance—it needs to be regularly checked. This is done in the MeerKAT operations. Relatively simple methods have

been used in the intra-MeerKAT time transfer and where physical hardware can be checked via a traceable measurement method.

This paper illustrates that sub-5-ns time tracking of the MeerKAT timing edge called the KTT is possible using GPS ($K^{(j)}_{\mathrm{GPS}}$) and are provided to the users in the TEMPO2 clock file format. These clock files were compared to KTT-UTC via using processing via the Observatoire de Paris and earlier processing with respect to the UTC(ZA) in Pretoria. The KTT timing is deterministically propagated to the telescope backend leading to very repeatable precise timing experiments that have been hitherto impossible, and it is conceivable that new types or ways of observation may be devised to measure either space object or earth-based parameters. Interferometers already play an important role in astrometry, and it could be possible that the capabilities of MeerKAT could make referencing to a celestial pulsar frame possible. There is also a project running to enable VLBI observations with MeerKAT that will also aid in this effort, and it could be possible that telescopes in Europe could also co-observe with the MeerKAT and its successor the SKA-MID.

It has been demonstrated for the first time that time transfer is possible, in a low noise and accurate manner using the PPP method, to the Paris Observatory. This data are well aligned to the UTC. The practical implication is that when referencing the KTT with respect to the UTC(OP) rather than the GPS time, the standard deviation in the resultant "KTT-UTC" sensor is reduced from slightly under 5 ns for GPS to ∼2.1 ns against UTC(OP) if significant effort is also put into calibration. A key beneficiating factor seems to be effective prediction and control of UTC(OP), apart from using a low-noise transfer method like PPP, which has less variations than a code only time transfer method. A laboratory that runs three masers and some cesium clocks like the NMISA can be shown to regularly achieve below the 10-ns level (peak deviation from UTC) with uncertainty to the UTC of smaller than 3 ns. The deviation from the UTC and the accuracy with which one can track the UTC(ZA) and the KTT is an often misunderstood aspect, as the important measure is how well is your offset known with respect to the UTC (at least for pulsar timing). The advantage of monitoring against the NMISA is in checking that the SARAO masers are stable as CV offers a fast 24 h check on SARAO masers. The UTC(OP) results are slower via PPP but more accurate and could therefore enable more accurate tracking on a 2 weekly basis than just the GPS time. Therefore, different institutes with different strengths can beneficiate the MeerKAT, apart from simply checking the result from the MeerKAT. Continued work and collaboration with both institutes are therefore recommended. The time tracking and timing uncertainty results reported in here could not have been obtained independently and show the importance of the BIPM and the clock nodes UTC(k) in supporting state-of-the-art scientific endeavors. South Africa's clock infrastructure has markedly improved in the last few years, with NMISA now operating nine atomic clocks in Pretoria,[96] and is able to sustain a combined uncertainty of 2.9 ns of the national UTC(ZA) node.

In order to maintain the requirements on timing, it will be required to have quarterly absolute calibrations. This is as GNSS receiver drift does take place and can sometimes appear suddenly.[97] There is ongoing work to pursue an absolute calibration of the GNSS time transfer receivers using a hardware simulation facility currently under construction, similar to work done at space agencies.[92,93,98] Furthermore, a calibrator that does not emit RFI is being built to transfer such calibration to site. Comparisons can also be done with GNSS receivers at National Metrology Institutes (NMI's) (keeping in mind there might be offsets in NMI's resulting in a 4.0-ns absolute calibration capability). If this regular calibration is not done, disturbing events or slow drift on the GNSS receivers can appear on the KTT-UTC products in TEMPO2. Finally, the MeerKAT backend and timing design could enable not just frequency but also timing comparisons as one way of future time transfer designs uses VLBI, in which there is ongoing interest.[99] For international telescope efforts, the usage of TWSTFT (at least in short periods between observations) could also be a consideration, possibly using a software defined ratio approach as used between the Physikalisch Technische Bundesanstalt (PTB) and the LNE-SYRTE at the Paris Observatory.[100,101] This work emphasizes that the natural symbiosis between GNSS and the UTC system[102] can be fortuitous-both are used by the MeerKAT. The GNSS at minimum form the basic part of high-accuracy time transfer to GPS and UTC(k). It is not inconceivable that a European laboratory or the SARAO might in fact be able to run a robust, and compact commercial cold atom clock or a robust mercury

ion clock[103] at the Losberg astronomy site[104] to further help to locally monitor/calibrate the masers, to ensure continued low uncertainty on a bi-weekly basis before the UTC is published.

9 Appendix A: Calculation of KTT's Uncertainty

9.1 *Initial Analysis Based on Measurement With Respect to NMISA*

An initial analysis of measurement uncertainty was done based on measurement with the NMISA[105] as per Fig. 10. The GPS system derives its time from the USNO and maintains its time close to the UTC. When no Circular T corrections are done for UTC(USNO), one gets an RMS difference of 2.56 ns between KTT-UTC as measured via the UTC(ZA) and $K_{\mathrm{GPS}}^{(1)}$ (of course neglecting unknown offsets), when the NMISA GNSS calibration was used. The measurements against the NMISA and comparison of the $K_{\mathrm{GPS}}^{(1)}$ against the KTT-UTC obtained in that way, implied that the GPS time was a worthy substitute of the UTC for monitoring.

One can find from the BIPM's Circular T that in the period of modified Julian dates spanning 58,990 to 59,160 (that was a half year up to March of this year) the UTC(USNO) was always <2 ns away from the UTC. This is suggesting one could naively estimate a uniform distribution between −2 and 2 ns at present for the differences between the UTC and the UTC(USNO), meaning a standard deviation of 1.15 ns with respect to the UTC.

Furthermore, data from the USNO[82] show that 1 month smoothed GPS time falls within 1 ns from the UTC(USNO) from 2015 to 2020. In calculations, it was assumed that one should rather use conservative +2 to −2 ns bounds for month long averaging of the GPS time, which means also a 1.15 ns RMSD between the UTC(USNO) and the GPS time. Clearly, the uncertainty that can be obtained via the GPS time then depends on the length of smoothing filter. In analysis, it was assumed that the GPS noise is $\sim 1/\sqrt{N}$, where N is the number of measurement/data points. One is therefore likely to get two times larger deviation between the GPS time and the UTC(USNO) in a week of averaging versus a month of averaging. This is as only $1/4$ of a month data points are used in a week as compared to a month. Under the assumption of white noise differences between the GPS time and the UTC(USNO), one obtains a 2.3-ns RMSD between the GPS time and UTC(USNO): this is given the symbol $u_{\mathrm{USNO,GPS}}$. This suggested that the uncertainty of $K_{\mathrm{GPS}}^{(1)}$ could be calculated as

$$\begin{aligned} u_{\text{KTT-GPS}} &= \sqrt{u_{\mathrm{sys,SARAO}}^2 + u_{\mathrm{sys,USNO}}^2 + u_{a,\mathrm{USNO}}^2 + u_{\mathrm{USNO,GPS}}^2} \\ &= \sqrt{4.1^2 + 1.5^2 + 0.2^2 + 2.3^2} \\ &= 5.41 \text{ ns}, \end{aligned} \tag{3}$$

where $u_{\mathrm{sys,USNO}}$ is the type B uncertainty and $u_{a,\mathrm{USNO}}$ the type A uncertainty for the UTC(USNO) stated in the BIPM's Circular T. (Assuming smoothing removes most measurement noise over a week, and assuming a $u_{\mathrm{sys,SARAO}}$ 4.1-ns KTT calibration uncertainty.) This is an overestimate as the GPS times does not have uniformly distributed noise. It is a scale that is steered towards the UTC and has correlation between samples/offsets during different dates, as was analyzed in the main manuscript.

9.2 *Accounting for Uncertainties in GNSS Receiver Calibration and Propagation Effects in System*

The calculation of the GPS receiver uncertainty follows the BIPM's methodology but does include extra components for the cables in the TFR, as the KTT is not directly measured by the GNSS receivers but through the extra ports of the masers. Furthermore, there is an uncertainty component for the cable used in the calibration kit that was shipped to other laboratories. The uncertainty components are shown in Table 3. The notation is similar to the Annexure 4 of the BIPM calibration GNSS procedure[106] and therefore the symbols and components u_i signifies uncertainties, with subscript b referring to type B uncertainties and subscript a to type A uncertainties as defined in the ISO/BIPM's guide to uncertainty in measurement.[107,108] The four columns marked P_1, P_2, $P_1 - P_2$, and P_3 represent uncertainties in delays associated with precision

Table 3 Uncertainty components related to a combination of GNSS and propagation delays through cables and components in the MeerKAT TFR. R_x refers to geodetic time transfer receivers and KTT PDA to the output of the overall TFR time pulses as used by the telescope, and which serves as the reference point for the rest of systems.

Uncertainty	P_1 (ns)	P_2 (ns)	$P_1 - P_2$ (ns)	P_3 (ns)	Description
u_b(travel)				4.0	Uncertainty of traveling receiver (including local effects)
Uncertainty contributed to the KTT from the clock side to the traveling R_x					
$u_{b,21}$	0.29	0.29	0	0.29	REFDLY$_T$ (at Losberg)
Uncertainties in delays: clock to GNSS receiver and the KTT reference point					
$u_{b,31}$	0.29	0.29	0	0.29	REFDLY$_R$ (at Losberg)
$u_{b,32}$	0.37	0.37	0	0.37	Delay uncertainty (KTT PDA output)
Uncertainties in antenna cable delays that must be measured in calibration kit					
$u_{b,41}$	0.2	0.2	0	0.2	Delay uncertainty of R_x cable
$u_{b,\mathrm{TOT}}$				4.05	For GPS, cables (at KTT PDA)
$u_{a,\mathrm{TOT}}$	0.01	0.435		0.7	RAWDIF (traveling R_x)
u_{CAL}				4.1	Quadrature sum: $u_{a,\mathrm{TOT}}$ and $u_{b,\mathrm{TOT}}$

GPS codes and their combinations. The GNSS calibration itself is based on the procedures as per the Annexure 1[109] and Annexure 3[110] of the BIPM procedure, although misclosure is estimated and not separately measured and not necessary when using the uncertainty as stated. Multipath and uncertainty in position is also neglected at this uncertainty level. It needs to be noted that two different calibrations as done first against the NMISA and then against LNE-SYRTE only gave a P_3 difference of 1.54 ns in the output of the VTSS. This also gives some idea of closure, as the NMISA obtained calibration via the PTB. The SARAO calibration is bracketed by two different UTC(k) receiver calibrations. $u_{b,21}$, $u_{b,31}$, and $u_{b,32}$ are derived from the uncertainties in measurements and measurement methods as described in Sec. 6.3. The calibration as shown in Table 3 specifically used a relative calibration with respect to the OP at this stage, and the value of uncertainty in the travelling calibrator is 4.0 ns if absolute calibration is referred to (that is when monitoring with somebody else apart from the OP as was done here). The variation RAWDIF of the traveling receiver (R_x) refers to diurnals either seen in the cable and/or antenna.

9.3 *Measurement to Other References and Possible Future Uncertainty*

When measuring to other references, one needs to take into account both the noise/stability and offset of the time standard that is used and also the noise/stability of the method of transfer. Ultimately, one would like to compare your local timescale to the UTC as it is the best kept international standard for timing. It is not necessarily simple to do so, and furthermore there is quite a big latency in the production of the BIPM Circular T. The need for accurate timing is on a bi-weekly basis in the case of the MeerKAT's observation program. Therefore, it is useful to work with predictions of the UTC, in which three was used in this work, that is the UTC(USNO) through the GPS via CGGTTS processing, the UTC(OP) via RINEX and CGGTTS processing, and the UTC(ZA) via CGGTTS processing. It was clear from our work that PPP can do very good transfer over long distances. The transfer via the GPS (as viewed over each station) over long distance is the worst method, with the CV GPS method having intermediate noise in between the methods of PPP and using the GPS times directly.

It is interesting to look at the RMSD between SKA1-UTC(OP) (PPP) and SKA1-UTC, which really illustrates that the Paris Observatory can predict the UTC quite well and can monitor the SARAO masers with low uncertainty. It could be conceivable that the SARAO can use the

RINEX files in the future, as were done in these experiments. Noise and stability of the transfer method have to be considered. Let us assume that the transfer via PPP has a stability of u_{PPP} of 1.0 ns (to account for shifts that can take place in the receivers on both side in between calibrations). Let us also assume it is possible in the future for the SARAO to have a calibration uncertainty of $u_{\mathrm{sys,KTT}} = 1.3$ ns (this could mean measures like adding a third receiver with a separate antenna directly on the KTT).

Then it would be possible to have a future uncertainty of

$$u_{\mathrm{KTT\text{-}UTC}} = \sqrt{u_{\mathrm{PPP}}^2 + u_{\mathrm{sys,OP}}^2 + u_{a,\mathrm{OP}}^2 + u_{\mathrm{sys,KTT}}^2} = 2.1 \text{ ns}, \tag{4}$$

when current values from the Circular T for OP is used. Clearly, this meets and exceeds SARAO requirements, and data could still be made available to the users even when referring to the UTC(OP) due to the closeness (small RMSD) between SKA1-UTC(OP) (PPP) and SKA1-UTC. Therefore even if the KTT could be smoothly steered to something close to UTC (for whatever reasons thought necessary) one can seemingly get excellent monitoring of KTT and therefore low uncertainty in timing.

Acknowledgments

The MeerKAT telescope has been built by the South African Radio Astronomy Observatory via South African public funds administered by the National Research Foundation, under the auspices of the Department of Science and Innovation (formerly under the Department of Science and Technology). The authors would like to thank the collaboration and support from the National Metrology Institute of South Africa (NMISA), and specifically Mr. Chris Matthee for various interactions over the years, as well the exchange of CGGTTS files up till this stage. The NMISA is funded by the South African Department of Trade and Industry. Dr. P. Tavella of the BIPM's Time Department is thanked for technical advice related to GNSS calibration and the reporting of the GNSS in the circular T among other things and discussion regarding comparison data related to GNSS, the UTC(USNO), and the UTC(SU), as well as general information on the UTC system. Gratitude is expressed to Dr. G. Petit of the BIPM's Time Department for communication on GNSS time transfer receiver triggering. The reviewers and associate editor are thanked for feedback and comments in order to improve this manuscript.

References

1. J. L. Jonas and MeerKAT Team, "The MeerKAT radio telescope," in *MeerKAT Sci.: On the Pathway SKA, Proc. Sci.* (2016).
2. I. Heywood et al., "Inflation of 430-parsec bipolar radio bubbles in the Galactic Centre by an energetic event," *Nature* **573**, 235–237 (2019).
3. W. D. Cotton et al., "Hydrodynamical backflow in X-shaped radio galaxy PKS 2014-55," *Mon. Not. R. Astron. Soc.* **495**, 1271–1283 (2020).
4. J. Delhaize et al., "MIGHTEE: are giant radio galaxies more common than we thought?" *Mon. Not. R. Astron. Soc.* **501**, 3833–3845 (2021).
5. Z. N. Khangale et al., "A spectroscopic, photometric, polarimetric, and radio study of the eclipsing polar UZ Fornacis: the first simultaneous SALT and MeerKAT observations," *Mon. Not. R. Astron. Soc.* **492**, 4298–4312 (2020).
6. M. Bailes et al., "The MeerKAT telescope as a pulsar facility: System verification and early science results from MeerTime," *Publ. Astron. Soc. Aust.* **37**, e028 (2020).
7. M. Kramer et al., "The relativistic binary programme on MeerKAT: science objectives and first results," *Mon. Not. R. Astron. Soc.* **504**, 2094–2114 (2021).
8. A. Ridolfi et al., "Eight new millisecond pulsars from the first MeerKAT globular cluster census," *Mon. Not. R. Astron. Soc.* **504**, 1407–1426 (2021).
9. A. Parthasarathy et al., "Measurements of pulse jitter and single-pulse variability in millisecond pulsars using MeerKAT," *Mon. Not. R. Astron. Soc.* **502**, 407–422 (2021).
10. R. M. Shannon et al., "Limitations in timing precision due to single-pulse shape variability in millisecond pulsars," *Mon. Not. R. Astron. Soc.* **443**, 1463–1481 (2014).

11. R. Deane, "News note: SA-MPG collaboration on extending MeerKAT," *Mon. Not. Astron. Soc. South Africa* **78**, 39–40 (2019).
12. G. Wieching, "MeerKAT extension (MK+) project overview," 2019, https://indico.skatelescope.org/event/551/attachments/5851/8631/.
13. Department of Communications and Science Engagement of the South African Radio Astronomy Observatory, "Media release: SARAO and the Max-Planck-Gesellschaft welcome the Italian Istituto Nazionale di Astrofisica as partner on the MeerKAT extension project," 2020, https://www.sarao.ac.za/media-releases/sarao-and-the-max-planck-gesellschaft-welcome-the-italian-istituto-nazionale-di-astrofisica-as-partner-on-the-meerkat-extension-project/.
14. G. P. Swart and P. Dewdney, "Highlights of the SKA1-Mid telescope architecture," *Proc. SPIE* **11450**, 114502T (2020).
15. A. Pellegrine et al., "MID-radio telescope, single pixel feed packages for the square kilometer array: an overview," *IEEE J. Microwaves* **1**, 428–437 (2021).
16. J. Burger et al., "Architecture for sensing of small clock shifts in Karoo Telescope Time on the MeerKAT GHz radio telescope," *Proc. SPIE* **11043**, 110431B (2019).
17. R. Siebrits et al., "Dissemination of reference signals for a next generation radio telescope," in *IEEE Int. Freq. Control Symp.*, pp. 1–6 (2018).
18. M. Bailes et al., "Multifrequency observations of SGR J1935+2154," *Mon. Not. R. Astron. Soc.* **503**, 5367–5384 (2021).
19. J. Zhang et al., "Analog–digital conversion signal-to-noise ratio analysis for synthetic aperture interferometric radiometer," *J. Appl. Remote Sens.* **8**(1), 083635 (2014).
20. B. Alachkar, A. Wilkinson, and K. Grainge, "Frequency reference stability and coherence loss in radio astronomy interferometers application to the SKA," *J. Astron. Instrum.* **7**(1), 1850001 (2018).
21. J. P. W. Verbiest et al., "Timing stability of millisecond pulsars and prospects for gravitational-wave detection," *Mon. Not. R. Astron. Soc.* **400**, 951–968 (2009).
22. R. P. Deane et al., "A close-pair binary in a distant triple supermassive black hole system," *Nature* **511**, 57–60 (2014).
23. R. P. Eatough et al., "A strong magnetic field around the supermassive black hole at the centre of the Galaxy," *Nature* **501**, 391–394 (2013).
24. K. Liu et al., "Pulsar-black hole binaries: prospects for new gravity tests with future radio telescopes," *Mon. Not. R. Astron. Soc.* **445**, 3115–3132 (2014).
25. D. Singh, K. Wu, and G. E. Sarty, "Fast spinning pulsars as probes of massive black holes' gravity," *Mon. Not. R. Astron. Soc.* **441**, 800–808 (2014).
26. P. Demorest and ngVLA Key Science Goal 4 Team, "ngVLA key science goal 4: fundamental physics with galactic center pulsars," *Bull. AAS* **53** (2021).
27. F. Tian et al., "Polynomial regression calculation of the Earth's position based on millisecond pulsar timing," *Res. Astron. Astrophys.* **12**, 219–234 (2012).
28. W. Becker, M. Kramer, and A. Sesana, "Pulsar timing and its application for navigation and gravitational wave detection," *Space Sci. Rev.* **214**, 1 (2018).
29. L. Li, L. Guo, and G.-L. Wang, "Detecting the errors in solar system ephemeris by pulsar timing," *Res. Astron. Astrophys.* **16**, 006 (2016).
30. A. Lyne et al., "Switched magnetospheric regulation of pulsar spin-down," *Science* **329**, 408–412 (2010).
31. A. Peens-Hough, "Time and frequency reference subsystem description and requirements," Tech. Rep. M0000-0000V1-42 TM Rev 2A, South African Radio Astronomy Observatory (2016).
32. W. Wenjun et al., "Two-way satellite time and frequency transfer: overview, recent developments and application," in *Eur. Freq. and Time Forum*, pp. 121–125 (2014).
33. J. P. Burger, "Pulsar and transient timing uncertainty allocation," Tech. Rep. MKAT-ECP-125, South African Radio Astronomy Observatory (2014).
34. Z. Jiang et al., "Improving two-way satellite time and frequency transfer with redundant links for UTC generation," *Metrologia* **56**, 025005 (2019).
35. J. Kouba and P. Hroux, "Precise point positioning using IGS orbit and clock products," *GPS Solutions* **5**(2), 12–28 (2001).

36. J. F. Zumberge et al., "Precise point positioning for the efficient and robust analysis of GPS data from large networks," *J. Geophys. Res. Solid Earth* **102**(B3), 5005–5017 (1997).
37. P. Héroux and J. Kouba, "GPS precise point positioning with a difference," Master's Thesis, University of New Brunswick (1995).
38. T. A. Clark, R. M. Hambly, and R. Abtahi, "Low-cost, high accuracy GPS timing," in *Proc. 13th Int. Tech. Meeting Satellite Division Inst. Navig.*, pp. 905–913 (2000).
39. A. E. E. Rogers and J. M. Moran, "Coherence limits for very-long-baseline interferometry," *IEEE Trans. Instrum. Meas.* **IM-30**(4), 283–286 (1981).
40. R. N. Manchester et al., "The Parkes pulsar timing array project," *Publ. Astron. Soc. Aust.* **30**, e017 (2014).
41. O. Terra and M. Hussein, "Accurate fiber length measurement using time-of-flight technique," *J. Opt. Commun.* **37**(2), 187–191 (2015).
42. U.S. Department of Commerce, "NIST/SEMATECH e-handbook of statistical methods," http://www.itl.nist.gov/div898/handbook/.
43. S. Ruffini, "ITU-T Q13/15, Network synchronization and time distribution performance," Joint IEEE 802 and ITU-T Study Group 15 Workshop, Geneva, Switzerland, 2020, https://www.itu.int/en/ITU-T/Workshops-and-Seminars/202001/Documents/Stefano_Ruffini.pdf.
44. E. Colard, "Distributing high-precision time over optical networks in the 5G world," https://www.gpsworld.com/distributing-high-precision-time-over-optical-networks-inthe-5g-world/ (accessed 20 June 2021).
45. E. G. Frankel, "Reliability of series and parallel systems," in *Systems Reliability and Risk Analysis*, Engineering Applications of Systems Reliability and Risk Analysis, Vol. 1, pp 33–63, Springer, Dordrecht (1988).
46. Z. Yu and Z. Li, "Best master clock algorithm of precision clock synchronization protocol," *Dianli Zidonghua Shebei (Electric Power Automation Equipment)* **29**, 74–77 (2009).
47. G. Adams, "PTP acceptance test report for serial numbers 05592 and 13445," Tech. Rep. M1300-0000-032 Revision 1, South African Radio Astronomy Observatory (2018).
48. T. V. Balla, "Acceptance test report: antenna positioner—time and frequency reference interface," Tech. Rep. M1300-0000-032 Rev 1, South African Radio Astronomy Observatory (2015).
49. A. R. Foley et al., "Engineering and science highlights of the KAT-7 radio telescope," *Mon. Not. R. Astron. Soc.* **460**(2), 1664–1679 (2016).
50. R. Siebrits et al., "Design of a low cost, compact round-trip delay measurement system for radio telescope time transfer applications," in *IEEE Int. Freq. Control Symp.*, pp. 1–4 (2016).
51. R. Siebrits et al., "Verification measurements of the Karoo array timing system: a laser radar based time transfer system," *Proc. SPIE* **10036**, 1003610 (2017).
52. International GNSS Service (IGS), RINEX Working Group and Radio Technical Commission for Maritime Services Special Committee 104 (RTCM-SC104), "The receiver independent exchange format," 2015, https://files.igs.org/pub/data/format/rinex303.pdf (accessed 25 June 2021).
53. P. Defraigne and G. Petit, "Time transfer to TAI using geodetic receivers," *Metrologia* **40**, 184–188 (2003).
54. P. Defraigne and G. Petit, "CGGTTS-version 2e: an extended standard for GNSS time transfer," *Metrologia* **52**, G1–G1 (2015).
55. D. Allan and M. Weiss, "Accurate time and frequency transfer during common-view of a GPS satellite," in *Proc. 34th Ann. Freq. Control Symp.*, Ft. Monmouth, NJ (1980).
56. K. Verhasselt and P. Defraigne, "Multi-GNSS time transfer based on the CGGTTS," *Metrologia* **56**, 065003 (2019).
57. J. Levine, "The statistical modeling of atomic clocks and the design of time scales," *Rev. Sci. Instrum.* **83**(2), 021101 (2012).
58. R. W. Schafer, "On the frequency-domain properties of Savitzky–Golay filters," in *Proc. Digital Signal Process. and Signal Process. Education Meeting*, pp. 54–59 (2011).
59. M. A. Little and N. S. Jones, "Generalized methods and solvers for noise removal from piecewise constant signals. I. Background theory," *Proc. Math. Phys. Eng. Sci.* **467**(2135), 3088–3114 (2011).

60. R. T. Edwards, G. B. Hobbs, and R. N. Manchester, "TEMPO2, a new pulsar timing package—II. The timing model and precision estimates," *Mon. Not. R. Astron. Soc.* **372**, 1549–1574 (2006).
61. M. Heflin et al., "Automated estimation and tools to extract positions, velocities, breaks, and seasonal terms from daily GNSS measurements: illuminating nonlinear Salton trough deformation," *Earth Space Sci.* **7**(7), e2019EA000644 (2020).
62. C. Munghemezulu, "Determination of geodetic velocity field parameters for the African tectonic plate using the technique of Global Navigation Satellite Systems," Master's Thesis, Faculty of Natural and Agricultural Sciences, University of Pretoria, Pretoria, South Africa (2013).
63. G. Petit, "Progresses in the calibration of geodetic like GPS receivers for accurate time comparisons," in *Proc. 15th Eur. Freq. and Time Forum*, Swiss Foundation for Research in Microtechnology, Neuchatel, Switzerland (2001).
64. "BIPM guidelines for GNSS calibration," 2016, https://webtai.bipm.org/ftp/pub/tai/publication/gnss-calibration/guidelines/ (accessed 22 June 2021).
65. K. Kalliomaki, J. Mannermaa, and T. Mansten, "Applicability of coaxial cables at picosecond range timing," in *Proc. 20th Eur. Freq. and Time Forum*, pp. 499–502 (2006).
66. G. D. Rovera et al., "Time delay measurements: estimation of the error budget," *Metrologia* **56**, 035004 (2019).
67. C. Shakarji, "Least-squares fitting algorithms of the NIST algorithm testing system," *J. Res. Natl. Inst. Stand. Technol.* **103**, 633 (1998).
68. I. Markovsky and S. Van Huffel, "Overview of total least-squares methods," *Signal Process.* **87**(10), 2283–2302 (2007). Special Section: Total Least Squares and Errors-in-Variables Modeling.
69. C. L. Sabharwal and B. Anjum, "Data reduction and regression using principal component analysis in qualitative spatial reasoning and health informatics," *Polibits* **53**(53), 31–42 (2016).
70. M. H. Centre, "Fitting an orthogonal regression using principal components analysis," Documentation for Matlab R2021a: Statistics and Machine Learning Toolbox Documentation, 2021, https://www.mathworks.com/help/stats/fitting-an-orthogonal-regression-using-principal-components-analysis.html.
71. Keysight Technologies, "53200A series RF/universal frequency counter/timers datasheet," Keysight Technologies.
72. L. Bisdounis et al., "Switching response modeling of the CMOS inverter for sub-micron devices," in *Proc. Design, Automation and Test in Europe*, pp. 729–735 (1998).
73. Y. Wang and M. Zwolinski, "Analytical transient response and propagation delay model for nanoscale CMOS inverter," in *IEEE Int. Symp. Circuits and Syst.*, pp. 2998–3001 (2009).
74. V. Maheshwari et al., "A novel method for delay analysis of CMOS inverter with on-chip RLC interconnect load," in *5th Int. Conf. Comput. and Devices Commun.*, pp. 1–3 (2012).
75. B. Nikolic, "Digital integrated circuits," 1999, Course Notes for Course EE141, University of California, Berkeley, http://bwrcs.eecs.berkeley.edu/Classes/icdesign/ee141f01/notes.html.
76. S. Hronik, "3.3 volt logic characteristics and applications," Renesas (2019).
77. M. Lombardi et al., "Time and frequency measurements using the global positioning system (GPS)," *Cal. Lab. Int. J. Metrol.* **8**, 26–33 (2001).
78. G. D. Rovera et al., "A simple computation technique for improving the short term stability and the robustness of GPS TAIP3 common-views," in *Joint Eur. Frequency and Time Forum Int. Frequency Control Symp.*, pp. 827–830 (2013).
79. G. D. Rovera et al., "UTC(OP) based on LNE-SYRTE primary frequency standards: five years of continuous operation," in *Conf. Precis. Electromagn. Meas.*, pp. 1–2 (2018).
80. W. Riley, "Handbook of frequency stability analysis," Tech. Rep. NIST Special Publication 1065, U.S. Department of Commerce (2008).
81. D. Matsakis, "Time and frequency activities at the U.S. Naval Observatory," *Int. J. Navig. Obs.* **2008**, 387418 (2008).

82. S. Mitchell, "USNO report to the GSIC timing subcommittee," 2019, https://www.gps.gov/cgsic/meetings/2019/mitchell.pdf.
83. I. Farrance and R. Frenkel, "Uncertainty of measurement: a review of rules for calculating uncertainty components through functional relationships," *Clin. Biochem. Rev.* **33**, 49–75 (2012).
84. R. K. R. Kessel, "Correlation in uncertainty of measurements—a discussion of state of the art techniques," in *XIX IMEKO World Congr., Fundamental and Appl. Metrol.* (2009).
85. F. E. Grubbs, "On estimating precision of measuring instruments and product variability," *J. Am. Stat. Assoc.* **43**(242), 243–264 (1948).
86. G. Li et al., "Using IGS RTS products for real-time subnanosecond level time transfer," in *China Satellite Navigation Conference (CSNC) 2018 Proceedings, Volume I*, J. Sun, C. Yang, and S. Guo, Eds., Springer, Singapore (2018).
87. D. Lyu, F. Zeng, and X. Ouyang, "Real-time PPP time transfer with ambiguity resolution," in *IEEE 4th Adv. Inf. Technol., Electron. and Autom. Control Conf.*, Vol. 1, pp. 824–828 (2019).
88. Y. Ge et al., "Enhancing real-time precise point positioning time and frequency transfer with receiver clock modeling," *GPS Solut.* **23**, 1–14 (2019).
89. O. P. Rønningen and M. Danielson, "A novel PPP disciplined oscillator," in *Joint Conf. IEEE Int. Freq. Control Symp. and Eur. Freq. and Time Forum*, pp. 1–4 (2019).
90. M. Ouyang et al., "Research on time and frequency transfer during PPP convergence with parameters correlation comparison," *Measurement* **173**, 108597 (2021).
91. J. Plumb et al., "Absolute calibration of a geodetic time transfer system," *IEEE Trans. Ultrason. Ferroelectr. Freq. Control* **52**(11), 1904–1911 (2005).
92. G. Ulrich et al., "Absolute calibration of time receivers with GPS/Galileo HW simulator," in *Proc. Eur. Time and Freq. Forum* (The 2008 Toulose Space Show) (2008).
93. D. Valat and J. Delporte, "Absolute calibration of timing receiver chains at the nanosecond uncertainty level for GNSS time scales monitoring," *Metrologia* **57**, 025019 (2020).
94. ISO/IEC JTC 1/SC 7 Software and systems engineering technical committee and IEEE Software & Systems Engineering Standards Committee (S2ESC), "ISO/IEC/IEEE international standard—systems and software engineering—system life cycle processes," ISO/IEC/IEEE 15288 First edition 2015-05-15, pp. 1–118 (2015).
95. T. Parker, "Environmental factors and hydrogen maser frequency stability," *IEEE Trans. Ultrason. Ferroelectr. Freq. Control* **46**, 745–751 (1999).
96. H. van de Groenendaal, "The science of accurate time," in *EngineerIT*, pp. 7–8, EIA Publishing (Pty) Ltd., Johannesburg (2021).
97. Z. Jiang, D. Matsakis, and V. Zhang, "Long-term instability in UTC time links," in *Proc. 48th Annu. Precise Time and Time Interval Syst. and Appl. Meeting*, pp. 105–126 (2017).
98. J. Ray and K. Senior, "Geodetic techniques for time and frequency comparisons using GPS phase and code measurements," *Metrologia* **42**, 215–232 (2005).
99. M. Sekido et al., "Broadband VLBI system using transportable stations for geodesy and metrology: an alternative approach to the VGOS concept," *J. Geod.* **95**, 41 (2021).
100. Y.-J. Huang et al., "Introduction of software-defined receivers in two-way satellite time and frequency transfer," in *IEEE Int. Freq. Control Symp.*, pp. 1–5 (2016).
101. Z. Jiang et al., "Use of software-defined radio receivers in two-way satellite time and frequency transfers for UTC computation," *Metrologia* **55**, 685–698 (2018).
102. G. Petit and P. Tavella, "Precise time scales and navigation systems: mutual benefits of timekeeping and positioning," *Satell. Navig.* **1**, 10 (2020).
103. E. A. Burt et al., "Demonstration of a trapped-ion atomic clock in space," *Nature* **595**, 43–47 (2021).
104. B. Pelle et al., "Cold-atom-based commercial microwave clock at the 10^{-15} level," in *IEEE Int. Freq. Control Symp.*, pp. 1–5 (2018).
105. J. P. Burger, R. S. Siebrits, and R. G. Gamatham, "Analysis and reporting of uncertainty related to time tracking of the clocks and clock distribution for the MeerKAT," Tech. Rep. M1300-0000-041 Revision 1, SARAO (2021).

106. BIPM Time Department, "Annex 4: template for the calibration report (BIPM Guidelines for GNSS equipment calibration—Annex 4)," 2015, webtai.bipm.org/ftp.
107. W. Kessel, "Measurement uncertainty according to ISO or BIPM -GUM," *Thermochim. Acta* **382**, 1–16 (2002).
108. Working Group 1 of the Joint Committee for Guides in Metrology (JCGM/WG 1), "JCGM 100:2008 GUM 1995 with minor corrections: evaluation of measurement data—Guide to the expression of uncertainty in measurement," 2008, www.bipm.org.
109. L. Tisserand and BIPM Time Department, "Annex 1: operational procedures for a visit of the traveling equipment (BIPM guidelines for GNSS equipment calibration—Annex 1)," 2021, webtai.bipm.org/ftp/pub/tai/publication/gnss-calibration/guidelines.
110. G. Petit and L. Tisserand, and BIPM Time Department, "Annex 3: procedure for computing raw difference of GNSS code measurements for geodetic receivers (BIPM guidelines for GNSS equipment calibration—Annex 3)," 2021, webtai.bipm.org/ftp/pub/tai/publication/gnss-calibration/guidelines.

Johan Petrus Burger received his BE and ME (both *cum laude*) degrees from the Rand Afrikaans University. He worked as a member of the technical staff at the Jet Propulsion Laboratory after receiving his PhD from the University of Southern California in 2001 and was an academic (teaching physics and doing laser research in Stellenbosch) and also worked at the National Metrology Institute Pretoria, South Africa. He is a functional manager of Time and Frequency Systems Group at the South African Radio Astronomy Observatory (SARAO).

Renier Siebrits received his MSc degree in electronic and electrical systems from ESIEE Paris and his MTech degree (*cum laude*) from the Cape Peninsula University of Technology as part of a dual master's degree program offered by the French South African Institute of South Africa. He is a senior hardware engineer of the Time and Frequency Systems Group at the South African Radio Astronomy Observatory, where he has been working since 2012.

Romeo Reginald Gunther Gamatham completed his undergraduate degree at the University of Namibia majoring in mathematics and physics. He then did his honors and master's degree in physics at the Nelson Mandela Metropolitan University (NMMU). His doctoral studies were centered around nonlinear effects in optical fibers at the Centre of Broadband Communication in the Physics Department of NMMU. He is currently working as a research scientist at NRF's SARAO.

Geomarr van Tonder completed her bachelor of electrical and electronic engineering and her master of electronic engineering degrees (*cum laude*) at Stellenbosch University, Stellenbosch, South Africa. She is a radio frequency engineer at the South African Radio Astronomy Observatory working within the Time and Frequency Reference Subsystem. She previously worked as an electronic frequency engineer at the Max Planck Institute for Radio Astronomy, Bonn, Germany.

Grant Adams received his BTech degree in electrical engineering from the Cape Peninsula University of Technology. He is a software and integration engineer at the South African Radio Astronomy Observatory. His main responsibilities are the integration and software/firmware development for the time and frequency systems. He has designed and implemented the local control and monitoring interfaces to MeerKAT TFR equipment, the TFR network architecture, and the core functionalities for the timing master controller.

Vereesé van Tonder received her BEng and MEng (*cum laude*) degrees in electronic engineering studies from Stellenbosch University in 2014 and 2012, respectively. She has been working as an electronics engineer since 2015 and is a member of the IEEE. In January 2017, she joined as a software engineer in the Electronics Functional Group, SARAO, Cape Town, South Africa.

Zwivhuya Ramudzuli received his BEng degree in computer engineering from the University of Pretoria and his MEng degree in electrical engineering from the University of Cape Town. While working on the time and frequency transfer systems, he developed a GPS time pulse radiator to independently verify the timing accuracy of the MeerKAT radio telescope receptors to universal coordinated time. He is a software engineer at the SARAO.

Sarah Buchner received her MSc degree in radio astronomy from Rhodes University. She is a science operations lead in the Science Operations Team at MeerKAT and a part of the multinational team for the MeerTIME pulsar timing program that uses MeerKAT for timing pulses from neutron stars. She previously worked at the Hartebeesthoek Radio Telescope and she was an Antarctic research officer at the University of Kwazulu-Natal.

Michel Abgrall received his PhD in 2003 in the characterization and operation of the FOM transportable atomic fountain from Laboratoire National de Metrologie et d'Essais (LNE-SYRTE). He is the head of National Reference Service Time at the LNE-SYRTE of the Time-Space Reference Systems part of the Paris Observatory responsible for developing reference standards in the time frequency. He has worked on space-based atomic clocks and aspects of improving fountain standards and their distribution. He was a co-winner of LNE Research Award in 2017.

Pierre Uhrich received his PhD in physics from the Louis Pasteur University, Strasbourg, France, in 1988 and he is a graduated engineer of the ENSMM, Besançon, France, in 1983. He is currently working in time and frequency metrology at LNE-SYRTE, Observatoire de Paris. He is part of the CCTF WG on GNSS. His main activities are about time transfer, time scale, stability, and the French contribution to EGNOS and Galileo.

Daniele Rovera received his "Laurea di dottore ingeneria elettronica" from the Politecnico di Torino in 1981. He is a research engineer at LNE. From 1981 to 1984, he worked at the Istituto Elettrotecnico Nazionale Galileo Ferraris on time transfer and had a small company for the realization of instruments dedicated to air sports. He has worked in various aspects of frequency chains and clock research at the LNE-SYRTE. He was a co-winner of the LNE Research Award in 2017.